University of California, San Diego UCSD-ENG-079

Assessment of Liquid Metal as the Divertor Surface of a Fusion Power Plant

Xiaobing Zhou[a,b] and Mark S. Tillack[a]

[a]University of California, San Diego
La Jolla, San Diego, CA 92093-0417, USA
[b]Southwestern Institute of Physics,
P.O.Box 432, Chengdu, 610041, P.R.China

January 1998

Fusion Division
Center for Energy Research

University of California, San Diego
La Jolla, CA 92093-0417

Assessment of Liquid Metal as the Divertor Surface of a Fusion Power Plant

Xiaobing Zhou[a,b] Mark S. Tillack[a]

[a]University of California, San Diego, La Jolla, San Diego, CA 92093-0417, USA
[b]Southwestern Institute of Physics, P.O.Box 432, Chengdu, 610041, P.R.China

January 1998

ABSTRACT

Economically competitive tokamak power plants require the divertor heat flux handling capacity to be as high as possible. Conventional solid surface divertors depend on impurity radiation or high recycling concepts to reduce the heat flux to about 5 MW/m^2. The liquid metal divertor is a promising candidate for handling high heat flux because of its unique properties of self-cooling, self-annealing and self-healing. In this report, the maximum divertor heat flux handling capacities of liquid divertor options are analyzed and design-oriented estimation is carried out based on typical tokamak experiments and power plant design parameters. Two methods are used to estimate the handling capacity, *i.e.*: i) constant impurity partial pressure between the divertor and core, and ii) empirical impurity compression factors at the divertor and scrape-off-layer. Two LM configurations are studied: film and droplet. Results show that the heat flux handling capacity of the LM divertor is related to the amount of impurities the core plasma can withstand, which is characterized in this work by the plasma effective charge Z_{eff}. If the increment of Z_{eff} due to LM impurity ranges from 0.1 to 0.5, then the maximum allowable heat flux is summarized as follows:

Heat Flux Limits (MW/m^2)

	constant pressure method	compression factor method
Ga Film	41.8–46.3	33.0–36.0
Ga Droplet	17.2–19.0	13.6–14.8
Li Film	48.5–58.3	25.0–29.3
Li Droplet	12.2–14.7	6.3–7.4

1. INTRODUCTION

With increasing interest in the design of an economically competitive fusion power plant [1–3], the problem of handling power load on the divertor will become more severe. To solve this problem, stationary solid surface divertor options seem to depend predominantly on the radiative mantle or radiative divertor to reduce the peak heat flux to about 5 MW/m^2 which the solid surface divertor can handle [4]. The possibility to sustain such a radiative mantle/divertor for steady state fusion reactor operation and its consistency with good core plasma performance is still in question. More work is needed before it can be established as the best candidate of divertor for a fusion power plant. Engineering design problems still exist for the stationary solid divertor. Such problems include plasma erosion, neutron-induced thermal conductivity degradation of target plate material, treatment of the inventory of tritium, damage of the surface by neutrons and runaway electrons, fatigue life, reliability of the joining of the plasma-facing tiles with heat sink material, *etc.* [5]

To handle the enormous charged particle power in a fusion power plant, a conventional divertor seems to be unsatisfactory, and a novel and robust divertor concept should be envisioned. Moving surface divertors are quite promising approaches for handling high heat flux in a fusion power plant. These include the continuous moving surface divertors such as the liquid metal (LM) film divertor [6] and the moving belt divertor [7], the surface of which is continuous, and the discontinuous moving divertor such as liquid metal droplet divertor [6].

The liquid metal (LM) divertor is attractive because of its unique properties of self-cooling, self-healing and self-annealing, which are very beneficial for the heat transfer requirements and divertor lifetime, which are two of the most serious issues in the design of a robust divertor. The use of liquid metal to supplant the solid material in the first wall dates back to 1971 by Christofilos [8]. The bold proposal to use liquid metal as heat flux receiver in a fusion reactor was made by the authors of the UWMAK design in 1973 [9]. A LM limiter was installed on the T-3M tokamak in 1985 [10]. The experiments on T-3M tokamak were not very successful but at least demonstrated the technical feasibility of a droplet curtain and sheet limiters and the compatibility of the gallium limiter with plasma discharge [11]. Investigations on hydrogen absorption and transport were carried out by Vodyanyuk *et al.* [12] and Liao *et al.* [13]. Simulated physical sputtering data showed that lithium is the most promising candidate material for LM divertor [14]. Liao *et al.'s* preliminary feasibility assessment showed, however, that the liquid gallium droplet curtain divertor is the most feasible based on tritium inventory, blistering erosion and MHD stability [15]. MHD stability problems of free surface liquid film in magnetic field (coplanar, vertical and oblique to flow plane) without surface-plasma boundary conditions taken into account were extensively

investigated [16]. The results showed that the magnetic field has a strong stabilizing effect on the film.

Operation of the divertor is one of the most serious issues in the design of a fusion reactor, especially for an economically competitive power plant in which the power core is very compact. In a device such as ARIES-ST, the space for the divertor is very limited while the transport heat power and particle flux in the SOL are large. To handle the enormous heat and particle flux of a spherical tokamak reactor, the conventional divertor (solid surface) will mainly depend on the complicated operation modes of the divertor. The most promising operation mode for such a conventional divertor concept is the completely-detached/partially-detached ELMy H-mode. Although different methods such as increasing the upstream mid-plane density, external injection of impurity, and increasing the connection length can now be used to obtain such kind of operation [17], the requirements for the detached operation are critical. The most commonly proposed tactic to obtain detachment is to radiate the outward plasma power before it reaches the divertor target by injecting externally some impurities as radiants. This method in fact complicates engineering design compatible with plasma operation in terms of the active control of injection and the design of injection loop.

The liquid metal divertor is a good option to handle such problems. It is not necessary for a LM divertor to operate at the completely detached/partially detached mode due to the intrinsic traits of self-annealing, self-healing, self-cooling and high handling capacity of heat flux which will be discussed below. Response to the plasma behavior may be self-controlled. Increase of plasma power to the SOL, and in turn the divertor plasma temperature, will result in higher temperature at the LM divertor surface. Higher surface temperature means higher saturated vapor pressure. Increase of evaporated liquid metal due to the elevated surface temperature will automatically increase the impurity density in the divertor chamber and SOL regions, and thus increase the radiated power and then decrease the temperature at the LM divertor surface. This self-adjusting process can play an important role in maintaining stable operation of the divertor, especially when abnormal events such as plasma ELM ejection or plasma disruption occurs. Lifetime of the LM divertor surface should not be affected by abnormal events due to the self-healing property of liquid metal. However, to determine the final design of the divertor, the operating point should be determined to keep the generation of liquid metal impurity in stable equilibrium with accumulation and exhaust of impurity in the plasma core. In the design of a spherical tokamak reactor, compactness is the main property. However, divertor space should be optimized by use of the requirements for exhaust of helium ash and the evaporated liquid metal.

The present report analyzes the maximum handling capacities of the divertor heat flux of both LM film concept and LM droplet curtain concepts [6]. Design-oriented estimates are made based on the typical parameters of present tokamak experiments and typical fusion power plant design parameters. In the estimation of handling capacity of divertor heat flux, the operational temperature of the liquid metal will be evaluated based on two methods. One is based on the assumption of constant impurity partial pressure, the other is based on the experimental results of enrichment of impurity in the divertor region. In Section 2, the handling capacity of divertor heat flux for LM film divertor option is estimated. The case for LM droplet curtain configuration is given in Section 3. Possible radiation fraction and the space needed for LM divertor in a compact tokamak reactor will be estimated based on the requirements for exhaust of helium ashes and the evaporated liquid metal is estimated in Section 4. Some tips on stable LM divertor options are discussed in Section 5. Discussion and conclusions are given in Section 6.

2. LIQUID METAL FILM DIVERTOR

In the tokamak edge, the radial distribution of the power flux in the scrape-off layer at mid-plane has the form [18]:

$$\Gamma(x) = \Gamma_o \, e^{(-r/\lambda_{mp})} \tag{2.1}$$

where r is the radial distance from the last closed flux surface, Γ_o is the peak heat flux and λ_{mp} is the decay length at the mid-plane. The plasma heat flux is taken as equivalent to a flux tube whose effective dimension is L_{eff}. Even though different methods are used to reduce the peak heat flux, they also widen its profile. Conservation of the total power results in the following expression for the average heat flux:

$$\Gamma_{HF} = \frac{\Gamma_0 \lambda_{mp}}{L_{eff}} \tag{2.2}$$

If the film flows through the plasma-swept region at an average speed v_{av}, the exposure time is $\tau = L_{eff}/v_{av}$ for a very thin (in the x-axis direction) slice of the moving surface as shown in Fig 2.1.

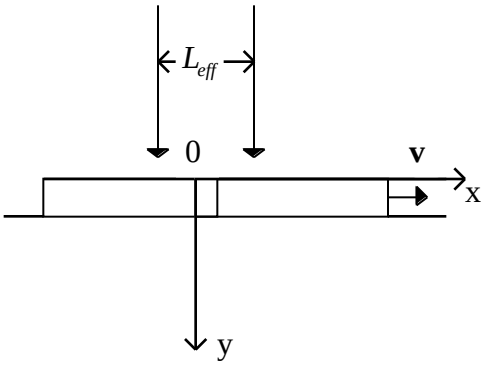

Fig. 2.1 Model of the LM film passing through the plasma heat flux.

Usually this time is very short due to the smallness of the tube and the rapidness of the flow. Every slice of the film will have the same exposure conditions, such that we can treat each slice as an isolated one. This assumption should not affect the final heat transfer results. Each slice moving through the heat flux tube for τ can be treated as if the slice is stationary and exposed to heat flux for τ. The film is assumed to be thick enough that it can be treated as semi-infinite. Then transient conduction in the liquid film is postulated to satisfy the following well-know one-dimensional transport equation with appropriate boundary and initial conditions [19]:

$$\frac{\partial T(y,t)}{\partial t} = \alpha \left(\frac{\partial^2 T(y,t)}{\partial y^2} \right) \tag{2.3}$$

(i)$T(0,t)=T_0$ for $t \le 0$

(ii)$T(y,t)$ for $y \ge \delta$

(iii)$\left. \frac{\partial T(y,t)}{\partial y} \right|_{y=0} = -\frac{\Gamma_{HF}}{\kappa}$

Solution of Eq.(2.3) when the film passes through the heat flux tube with exposure time τ can be obtained as follows:

$$T(y,t) = T_0 + \frac{\Gamma_{HF}\sqrt{\alpha}}{\kappa} \left[2\sqrt{\frac{t}{\pi}} e^{-y^2/4\alpha t} - \frac{y}{\sqrt{\alpha}} erfc\left(\frac{y}{2\sqrt{\alpha t}} \right) \right] \tag{2.4}$$

where T_o is the initial temperature, Γ_{HF} is the plasma heat flux, $\alpha=\kappa/\rho C_p$ is the thermal diffusivity of the LM film, κ is the thermal conductivity, C_p is the specific heat and ρ is the mass density, $erfc(x) = \frac{2}{\sqrt{\pi}} \int_x^\infty e^{-\xi^2} d\xi$ is the conjugate error function. The thickness of heating δ in the film is determined by:

$$f(\delta) = 2\sqrt{\frac{\tau}{\pi}} e^{-\delta^2/4\alpha\tau} - \frac{\delta}{\sqrt{\alpha}} erfc\left(\frac{\delta}{2\sqrt{\alpha\tau}} \right) = 0 \tag{2.5}$$

In order for the above analysis to be correct and to keep constant the temperature of the substrate under the film, the thickness of the film should not be thinner than δ. The potential of the LM film in handling the surface heat flux is governed by Eq.(2.4). Taking $T(0,\tau)=T_{op}$ (the operation temperature of the LM at the operation divertor pressure), $T_o=T_m$ (the melting point temperature), the peak heat flux that the LM film can handle is:

$$\Gamma_{HF}^{\max} = \frac{\kappa\left(T_{op} - T_m\right)}{2} \sqrt{\frac{\pi v_{av}}{\alpha L_{eff}}} \tag{2.6}$$

If the operating temperature is taken as the boiling point (2403˚C for gallium, 1371˚C for lithium, corresponding to the pressure of 1 atm) and L_{eff}=1m, and v_{av}=5 m/s, then $\Gamma_{HF}^{\max}$ =34.127 MW/m^2, δ=12.5 mm for gallium, and $\Gamma_{HF}^{\max}$ =28.923 MW/m^2, δ=18.5mm for lithium. In a tokamak reactor, the pressure at the divertor is usually smaller than 1 atm, therefore these maxima are only the topmost values for the estimation of the maximum handling capacity of heat flux by LM divertor.

The method for estimation of the handling capacity of heat flux of the moving belt divertor is treated the same as the film case. But the window of temperature for estimating the maximum capacity is from room temperature (taken as the same as the melting point of gallium in order to make comparison) to the melting point of the solid material. When the velocity of the moving belt and the effective width of the heat flux is the same as those discussed above as LM film divertor, $\Gamma_{HF}^{\max}$ =136.027 MW/m^2, δ=25.5mm for tungsten tiles and $\Gamma_{HF}^{\max}$ = 54.638 MW/m^2, δ=21.5 mm for beryllium tiles. Such thicknesses are larger than expected for liquid film concepts.

The effective length of the plasma heat flux at the divertor target surface is an important parameter in the determination of the allowable heat flux at the divertor target surface. It is usually determined by two factors. The first is the expansion of the magnetic flux tube from the mid-plane to the divertor region, not including the plate angle inclination. The second is the expansion due to physical process such as radiative divertor and/or gas puffing in the scrape-off layer and private region. If it is supposed that the expansion factor due to magnetic flux tube expansion is Q_m and the expansion factor due to radiative transport processes is Q_r, then the decay length at the divertor plate is:

$$\lambda = \lambda_{mp} Q = \lambda_{mp} Q_m Q_r \tag{2.7}$$

where Q is the total expansion factor, λ_{mp} is the decay length at the mid-plane. The radial profile of the heat flux just before the divertor surface is:

$$\Gamma(r) = \frac{\Gamma_0}{Q} e^{-r/(Q\lambda_{mp})} \tag{2.8}$$

while at the divertor surface which is tilted, the profile of the heat flux is:

$$\Gamma(x) = \Gamma_D e^{-x/\lambda_D} \tag{2.9}$$

where x is the distance from strike point along the divertor target surface. The peak heat flux at the divertor is $\frac{\Gamma_0 \sin\eta}{Q}$ with the decay length at the divertor surface being $Q\lambda_{mp}/\sin\eta$, where η is the glancing angle of the magnetic field line to the divertor surface. Γ_D can be estimated as [20]:

$$\Gamma_D = f_c P_{SOL} \sin(\eta)/2\pi R_s Q\lambda_{mp} \tag{2.10}$$

where f_c is the asymmetry coefficient between inner and outer legs of the divertor. For the symmetry case, f_c =0.5 for single null and 0.25 for double null configuration. Supposing the effective length is:

$$L_{eff} = Q\lambda_{mp}/\sin\eta \tag{2.11}$$

the divertor heat flux the film can handle takes the form:

$$\Gamma_D^{\max} = \frac{\kappa\left(T_{op} - T_m\right)}{2}\sqrt{\frac{\pi v_{av}\sin\eta}{\alpha\lambda_{mp}Q}} \tag{2.12}$$

which is obtained from Eq.(2.6) and $\int_0^\infty \Gamma(x)dx = \Gamma_{HF}L_{eff}$. This corresponds the normalized heat flux from Eq.(2.10):

$$\left(\frac{P_{SOL}}{R_S}\right)^{\max} = \frac{\pi\kappa\left(T_b - T_m\right)}{f_c}\sqrt{\frac{\pi v_{av}Q\lambda_{mp}}{\alpha\sin\eta}} \tag{2.13}$$

If η=15˚C, a typical design parameter for a fusion reactor [20], the scrape-off length at the mid-plane is λ_{mp}=1 cm and Q=5 which are typical values of the present experimental reactors [18], and if v_{av}= 5 m/s, then $\Gamma_D^{\max}$=77.64 MW/m^2 for gallium, 65.80 MW/m^2 for lithium. This means that with the heat flux expansion factor attainable at the present experimental reactors, the gallium film divertor with thickness ~5.5 mm has the potential to handle the divertor heat flux of 77.64 MW/m^2, while the lithium film divertor with thickness ~8.5 mm can handle a maximum of 65.80 MW/m^2 of divertor heat flux. Maximum handling capacity of divertor heat flux corresponds to the temperature window from the melting point to the boiling point (at 1 atm). In the realistic case of the operation of tokamak divertor, the working temperature window for gallium (lithium) is between the melting point of 29.8˚C (186˚C) and the saturation temperature which corresponds the saturated vapor partial pressure which the plasma operation can tolerate. If the saturation temperature of 750˚C (325˚C) is chosen for gallium and lithium according to Ref.[13], the normal handling capacity of divertor heat flux is then 23.56 MW/m^2 for gallium film and only 7.72 MW/m^2 for lithium film. However, the saturation temperature of 750˚C (325˚C) chosen as the operation temperature underestimates the normal handling capacities of liquid metal divertor from the following discussion. All these results are shown in Table 2.1. The critical issue is now the determination of the operational temperature of the liquid surface. Due to the uncertainty to correlate the liquid surface temperature to the core plasma properties, two methods are used in the following section.

For moving belt, Γ_D^{max}=309.5 MW/m^2 for tungsten tiles and 124.3 MW/m^2 for beryllium tiles for the parameters given in Table 2.1. The operation temperature limit of tungsten is 1500˚C and that of beryllium is 800˚C. The corresponding normal capacity is 136.20 MW/m^2 for tungsten tiles and 76.26 MW/m^2 for beryllium tiles.

Table 2.1 Estimated handling capacity of heat flux by use of constant pressure method

Expansion factor Q of SOL width from mid-plane to divertor		5
Scrape-off length at mid-plane λ_{mp}		1 cm
Surface moving speed v_{av}		5 m/s
Effective width of the heat flux tube $L_{eff} = Q\lambda_{mp}/\sin\eta$		0.193 m
Divertor target plate inclination angle η		15˚
Decay length of heat flux profile at target plate $\lambda_D = Q\lambda_{mp}/\sin\eta$		0.193 m
Maximum handling capacity of heat flux	Moving W-tile	309.47 MW/m^2
	Moving Be-tile	124.29 MW/m^2
	Ga-film	77.64 MW/m^2
	Ga-droplet	31.90 MW/m^2
	Li-film	65.80 MW/m^2
	Li-droplet	16.57 MW/m^2
Maximum thickness needed and droplet size	Moving W-tile	11.5 mm
	Moving Be-tile	9.5 mm
	Ga-film thickness	5.5 mm
	Ga-drop radius	4.3 mm
	Li-film thickness	8.5 mm
	Li-drop radius	10.7 mm
Plasma parameters (ARIES-RS)	Electron density n_e	2.11×10^{21}/m^3
	Ion temperature T_i	18.0 keV
Working temperature window for moving belt	Moving W-tile	(30.0–1500)˚C
	Moving Be-tile	(30.0–800)˚C
Working temperature window according Ref.(13)	Gallium	(29.8–750.0)˚C
	Lithium	(186–325.0)˚C
Normal handling capacity of divertor with above operational window	Moving W-tile	136.20 W/m^2
	Moving Be-tile	76.26 W/m^2
	Gallium film	23.56 MW/m^2
	Lithium film	7.72 MW/m^2

2.1 Heat flux handling capacity of LM film divertor by constant liquid metal partial pressure method

Generally, the operation temperature of the LM divertor should be determined by how much contamination the plasma can withstand by the liquid metal evaporated and eroded when interacting

with the plasma. We suppose that the erosion due to plasma-LM interaction is negligible and the contamination of plasma is due to the evaporated LM, which is determined by the saturated vapor pressure. The problem is how to correlate the density or partial pressure of impurity ions in the plasma core with the evaporated neutrals at the divertor surface, which is determined directly by the saturated vapor pressure. This is really a complicated problem. From the point of view of divertor target protection and low additional plasma contamination, a high ratio of $P_{rad}/\Delta Z_{eff}$ is preferred. This quantity is strongly influenced not only by the line averaged electron density and the edge electron temperature, but also by the transport region [21]. As there is no direct empirical relationship available, the impurity partial pressure of the LM is assumed to be the vapor pressure at the LM divertor here for our analyses.

The saturated vapor pressure of a chemical element is correlated by [22]:

$$\log(p) = A - \frac{B}{T} + CT + D\log(T) \tag{2.14}$$

where p is in Torr and T in ˚K. For gallium: A=9.635, B=13984, C=0.0, D=-0.3413 [23]. For lithium (liquid lithium, 180.7–1077˚C): A=12.9992, B=8442.53, 2.5968×10-4, D=–1.64038. For a 50/50 D-T power plant with the concentration of the helium ash being 10%, the relationship between the density of the impurity at the plasma core and the plasma effective charge is obtained from the definition of $Z_{eff.}$, *i.e.*:

$$n_{LM} = \frac{(Z_{eff} - 1.2)n_e}{Z_{LM}(Z_{LM} - 1)} \tag{2.15}$$

where Z_{LM} is the charge number of the liquid metal (as impurity in the plasma core) and n_e is the average electron density. The partial plasma pressure of the impurity is:

$$p_{LM} = n_{LM}\, kT_i \tag{2.16}$$

where T_i is the ion temperature at the core and the thermal equilibrium between the impurity ions and fuel ions is assumed. To estimate the operation temperature of the LM divertor surface, Eq.(2.16) is taken to be exactly the vapor pressure. The relations of the partial plasma pressure of the gallium ions and the gallium-ion concentration in the plasma with the effective charge of the core plasma Z_{eff} are shown in Fig.2.2, where parameters of the ARIES-RS power plant are used, *i.e.*, n_e=2.11×10^{20}/m^3, T_i=18.0 keV. The corresponding cases for lithium are shown in Fig.2.3. From the above figures we can see that the reactor plasma can withstand quite a large fraction of lithium and thus large partial pressure due to its low atomic number. This fact will increase greatly

the operation temperature of the lithium divertor. From Eqs.(2.14)-(2.16) the operation temperature is determined by the following equation:

$$CT + D\log T - \frac{B}{T} + A - \log\left[\frac{\left(Z_{eff} - 1.2\right)n_e kT_i}{Z_{LM}\left(Z_{eff} - 1\right)}\right] = 0 \tag{2.17}$$

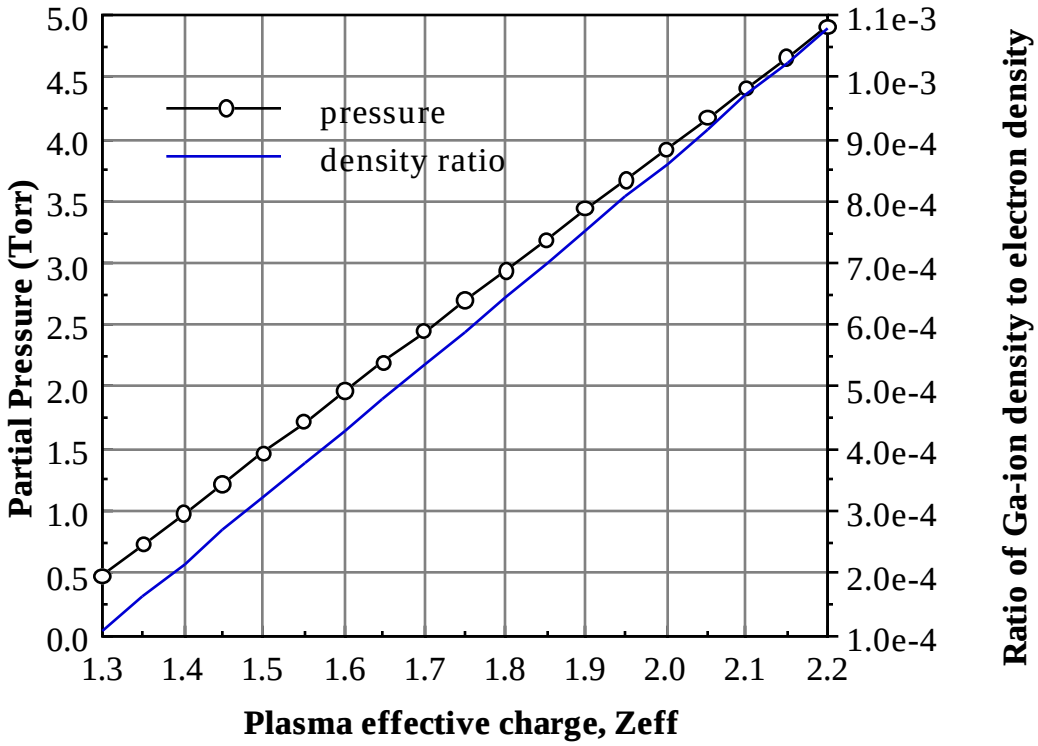

Fig 2.2 The partial pressure (Torr) and the ratio of the density of gallium ions as impurity in a reactor core with n_e=2.11×10^{20}/m^3, T_i=18.0 keV to the electron density versus the plasma effective charge Z_{eff}.

For a typical fusion power plant such as ARIES-RS, n_e=2.11×10^{20}/m^3, T_i=18.0 keV, solution of T versus Z_{LM} can be obtained for gallium or lithium. If the units for n_e, T_i, T and p are 10^{20}/m^3, keV, °K and Torr respectively, Eq.(2.17) becomes:

$$CT^2 + T\left\{A - \log\left[\frac{120.01\left(Z_{eff} - 1.2\right)n_e T_i}{Z_{LM}\left(Z_{LM} - 1\right)}\right]\right\} + DT\log T - B = 0 \tag{2.18}$$

The relationship between the normal operation temperature (°C) and the plasma effective chargeZ_{eff}. for gallium divertor and lithium divertor is shown in Fig.2.4 when the product of the electron density and the temperature of the ions $n_e kT_i = 37.98 \ \ (10^{20} m^{-3} keV)$.

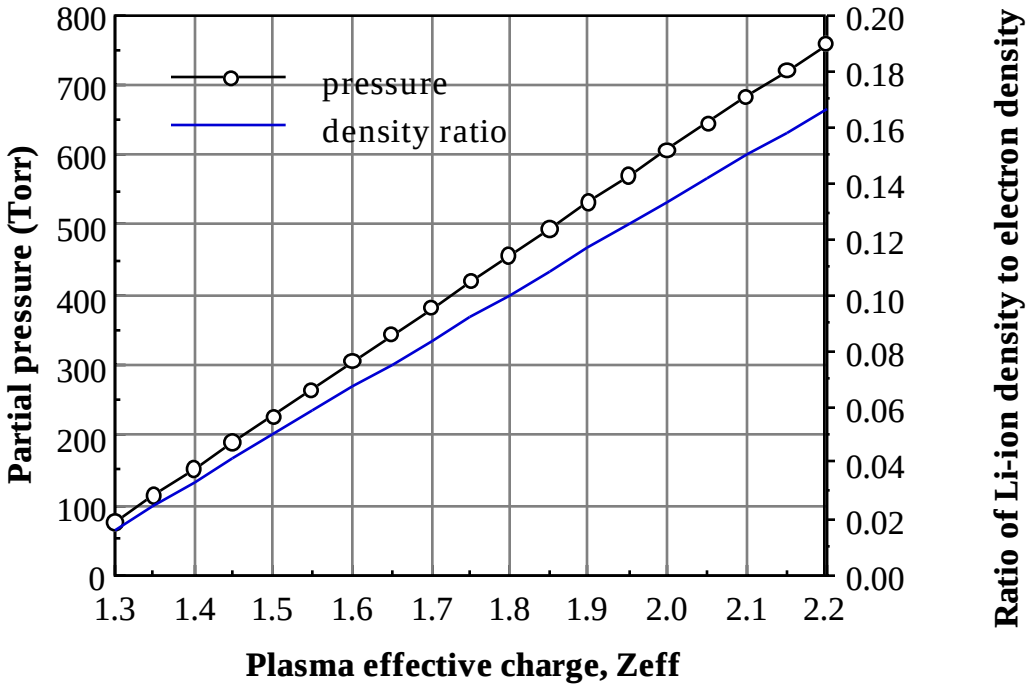

Fig 2.3 The partial pressure (Torr) and ratio of the density of lithium impurity ions in the core withn_e=2.11×10^{20}/m^3, T_i=18.0 keV to the electron density versus the plasma effective charge Z_{eff}

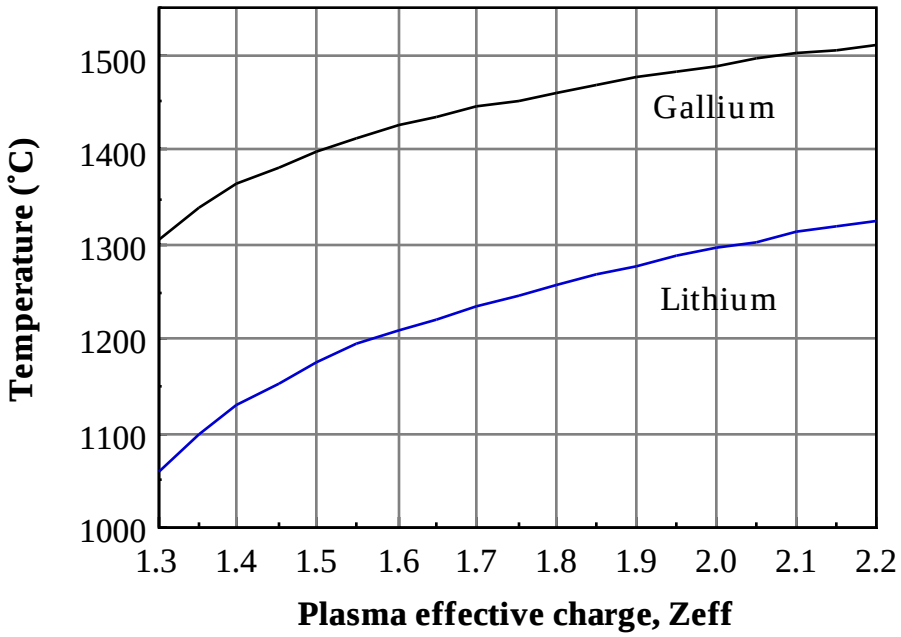

Fig. 2.4 The relationship between the normal operation temperature of liquid gallium divertor and lithium divertor at which the core of a fusion power plant can withstand the saturated vapor pressure of the liquid metal and the plasma effective charge Z_{eff}.

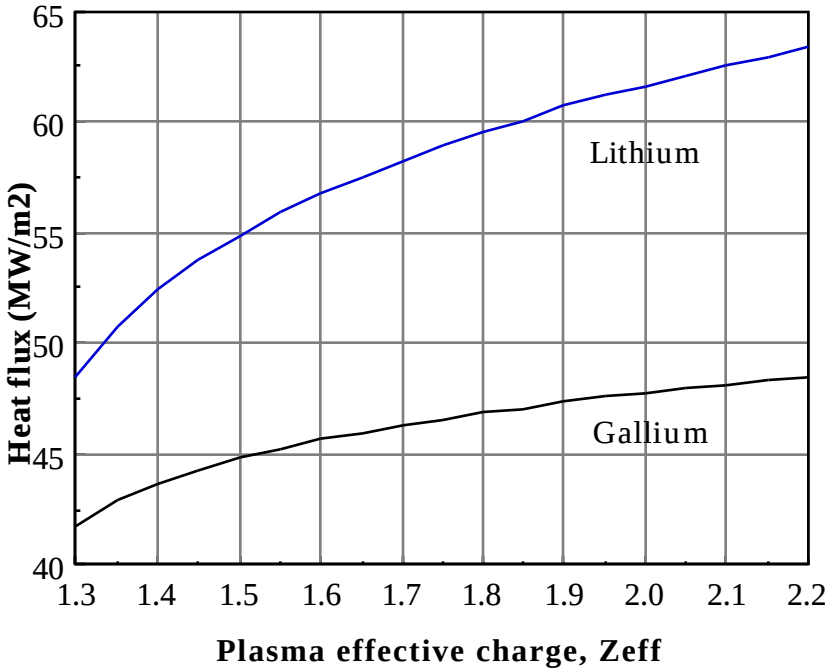

Fig. 2.5 The relationship of the normal handling capacity (MW/m^2) of divertor heat flux which the liquid gallium and lithium film divertors can handle at normal conditions with the plasma effective chargeZ_{eff}. for typical fusion plant parameters shown in Table 2.1.

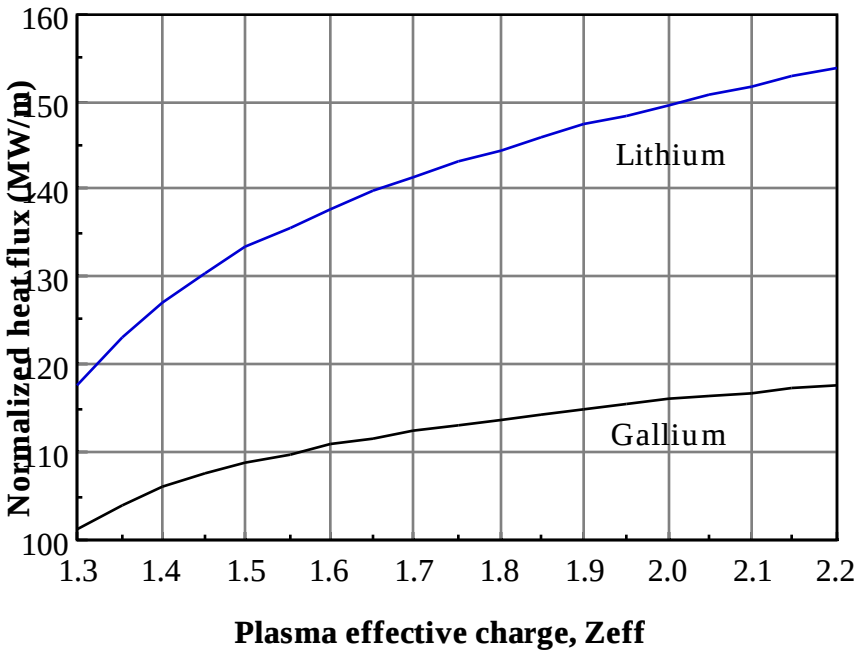

Fig. 2.6 The relationship of the normalized heat flux (MW/m) which the liquid gallium and lithium film divertors can handle at normal conditions with the plasma effective charge Z_{eff} for typical fusion plant parameters shown in Table 2.1.

From the above results we can see that for reasonable values of the plasma effective charge, the operating temperature of the liquid metal divertor is much higher than expected. This increment in the operation temperature apparently enlarges the operation range of temperature for the LM divertor. Combination of Eq.(2.12) with Eq.(2.17) can be solved numerically to obtain the normal handling capacity of divertor heat flux. The results are given in Fig.2.5 where typical reactor parameters are given in Table 2.1 and the plasma parameters of ARIES-RS are used.

Projection of the above results to the normalized heat flux according to Eq.(2.13) is shown in Fig.2.6 for the single null configuration. Comparison of the normal handling capacity of divertor heat flux shows that lithium is competitive with gallium. This is out of our expectation but it is understandable. The handling capacity is governed by $\kappa/\sqrt{\alpha}$ and the operation range of temperature. $\kappa/\sqrt{\alpha}$ is 12316.6 W-s$^{1/2}$/m^2-˚C for lithium, larger than 7256.6 W-s$^{1/2}$/m^2-˚C for gallium with the ratio being 1.7. While from Fig.2.4, the temperature range is 872.8˚C for lithium and 1276.6˚C for gallium with ratio being 1.46 when Z_{eff}=1.3. Therefore the results are comparable with or even larger than those of gallium.

Table 2.2 Estimated handling capacity of divertor heat flux

Plasma parameters	Electron density n_e		2.11×10^{21}/m^3
	Ion temperature T_i		18.0 keV
	Z_{eff}		1.3–1.4
Increase of Z_{eff} due to LM vapor	ΔZ_{eff}		0.1–0.2
Working temperature window	Gallium	ΔZ_{efff}=0.1	(29.8–1306.6)˚C
		ΔZ_{efff}=0.2	(29.8–1363.2)˚C
	Lithium	ΔZ_{efff}=0.1	(186–1058.8)˚C
		ΔZ_{efff}=0.2	(186–1129.5)˚C
Normal handling capacity of divertor	Ga-film		(41.77–43.63) MW/m^2
	Ga-drop		(17.16–17.92) MW/m^2
	Li-film		(48.47–52.39) MW/m^2
	Li-drop		(12.21–13.19) MW/m^2
Normalized heat flux P_{SOL}/R_s in case of SN configuration	Ga-film		(101.4–105.9) MW/m
	Ga-drop		(41.66–43.51) MW/m
	Li-film		(117.7-127.2) MW/m
	Li-drop		(29.63–32.03) MW/m
Saturated vapor pressure	Gallium		(0.49–0.98)Torr
	Lithium		(75.97–151.93)Torr
Impurity concentration in plasma core n_{LM}/n_e	Gallium		$(1.075-2.151)\times10^{-2}$%
	Lithium		1.667% –3.333%

For design purposes, Z_{eff}=1.3–1.4 which corresponds to ΔZ_{eff}=0.1–0.2 due to liquid metal saturated vapor is chosen in order to leave enough margin for other impurity-generation mechanisms. This consideration should be conservative with the results shown in Table 2.2.

2.2 Heat flux handling capacity of LM film divertor by compression factor for liquid metal method

How well the impurity, *i.e.*, LM vapor can be retained near the divertor is so important that the operation temperature of the LM divertor is eventually determined from it. Retention of the impurity can be more conveniently characterized by the compression ratio C_Z which is defined as the ratio of the neutral impurity density in the divertor region to the impurity ion density in the plasma core, *i.e.*

$$\begin{aligned} C_Z &= n_Z^{N,div} / n_Z^{i,coreedge} \\ &= \frac{P_Z^{N,div} T_Z^{i,core\ \ edge}}{P_Z^{i,core\ \ edge} T_Z^{N,div}} \\ &= C_Z^P / C_Z^T \end{aligned} \tag{2.19}$$

where C_Z^P is the ratio of the neutral impurity partial pressure at the divertor (the vapor pressure of LM) to the impurity ion partial pressure at the plasma core edge, usually evaluated at normalized minor radius ρ=0.7 for the ELMy H-mode operation plasma [23], C_Z^T is the ratio of the neutral impurity temperature at the divertor region to the impurity ion temperature at the plasma core edge. Thermal equilibrium between evaporated neutrals and the divertor plasma ions is assumed here. ρ=0.7 is chosen due to: i) ρ≤0.7 is the interior of ELM zone; ii) impurity is usually completely stripped for ρ≤0.7; iii) ρ=0.7 is still close enough to the plasma edge to respond quickly to the change of conditions at divertor.

A strong increase of impurity compression is observed as the neutral flux in the divertor region increases. The compression ratio is also quite species-dependent. Both results from codes and experiments show that the compression ratio of helium is lower than other impurities such as nitrogen. This is due to the higher ionization potential for helium than for nitrogen. For a neutral gas flux density of 1.2×10^{22} D_2 molecules/m^2s, the compression ratio for nitrogen is found to be 15 (±5) [24] from experiment and 20 from code. An increase in the neutral gas flux density can increase the compression factor. For gallium as the divertor surface material, the compression ratio should be even higher than that of nitrogen. To be conservative, it is supposed to be 20.

For lithium as the divertor surface material, the compression ratio should be a little higher than helium for which about 1.2 can be reached experimentally [25]. In the following discussion, the compression ratio for the lithium vapor at the divertor is chosen to be 2.0. A large compression ratio for impurity should be beneficial for the LM divertor operation from the point of view of contamination-resistance to the core plasma and increase of the operating temperature of the liquid metal. For ARIES-ST, the temperature at the magnetic axis is 13.1 keV, and the profile of the temperature is assumed to be:

$$T = T_0\left(1-\rho^2\right)^{\alpha_T} \quad (\alpha_T = 0.702) \tag{2.20}$$

From Eq.(2.19), the ratio of the LM vapor pressure to the LM impurity ion partial pressure at the plasma edge is:

$$C_Z^P = C_Z \; C_Z^T \tag{2.21}$$

For a liquid divertor concept, the divertor plasma temperature can be higher than for a solid surface divertor concept. If 10~50 eV is tolerable, then C_Z^P is 0.0245~0.1226 for gallium and 0.00245~0.01226 for lithium. The plasma ion pressure and density profiles are still supposed to be in the same form as Eq.(2.20) with α_P=1.174 and α_n=0.634. The ratio of the vapor pressure at the divertor to the average ion pressure in the plasma core is governed by:

$$\begin{aligned} C_Z^{P,ave} &= C_Z^P k_n k_T \left(1-\rho^2\right)^{\alpha_P}\Big|_{\rho=0.7} \\ &= C_Z C_Z^T k_n k_T \left(1-\rho^2\right)^{\alpha_P}\Big|_{\rho=0.7} \\ &= \frac{C_Z T_Z^{N,div}}{T_0} k_n k_T \left(1-\rho^2\right)^{\alpha_P-\alpha_T}\Big|_{\rho=0.7} \end{aligned} \tag{2.22}$$

where T_0 is the ion temperature at the plasma center, k_n and k_T are peak to average ratios for density and temperature respectively. Corresponding to the divertor plasma temperature of from 10 to 50 eV, it is 0.0169~0.0849 for gallium and 0.00169~0.00849 for lithium, where k_n=1.399, k_T=1.123 are used. The evaporation of the liquid metal is a local effect depending on the temperature of the surface of the LM divertor. The saturated vapor pressure of a chemical element is governed by Eq.(2.14). From the definition of $C_Z^{P,ave}$, the operation temperature of the liquid metal divertor is determined by the following equation which is analogous to Eq.(2.17):

$$CT + D\log T - \frac{B}{T} + A - \log\left[\frac{\left(Z_{eff}-1.2\right)n_e k T_i C_Z^{P,ave}}{Z_{LM}\left(Z_{eff}-1\right)}\right] = 0 \tag{2.23}$$

From above we can obtain the relationship of the operating temperature T with Z_{eff} which is shown in Fig.2.7, in which the average ion temperature is 11.66 keV, and the average electron density is 3.029×10^{20} m^{-3}. To see the effect of compression factor on the operating temperature, a case where the compression factor for lithium vapor is assumed increased to 20 – the same as the value for Ga – is shown in Fig.2.8. The saturated gallium vapor pressure at the divertor and the ratio of the average gallium ion density to the average electron density in the plasma core is shown in Fig.2.9. The corresponding case for lithium is shown in Fig.2.10. The normal handling capacity of the divertor heat flux of gallium and lithium film divertors versus the plasma effective charge Z_{eff} for the case that the compression ratio for lithium vapor at divertor is 2.0 is shown in Fig.2.11. The corresponding handling capacity of normalized divertor heat flux is given in Fig.2.12. The normal handling capacity of the divertor heat flux of gallium and lithium film divertors versus the plasma temperature T_{div} at divertor when Z_{eff} =1.7 is shown in Fig.2.13.

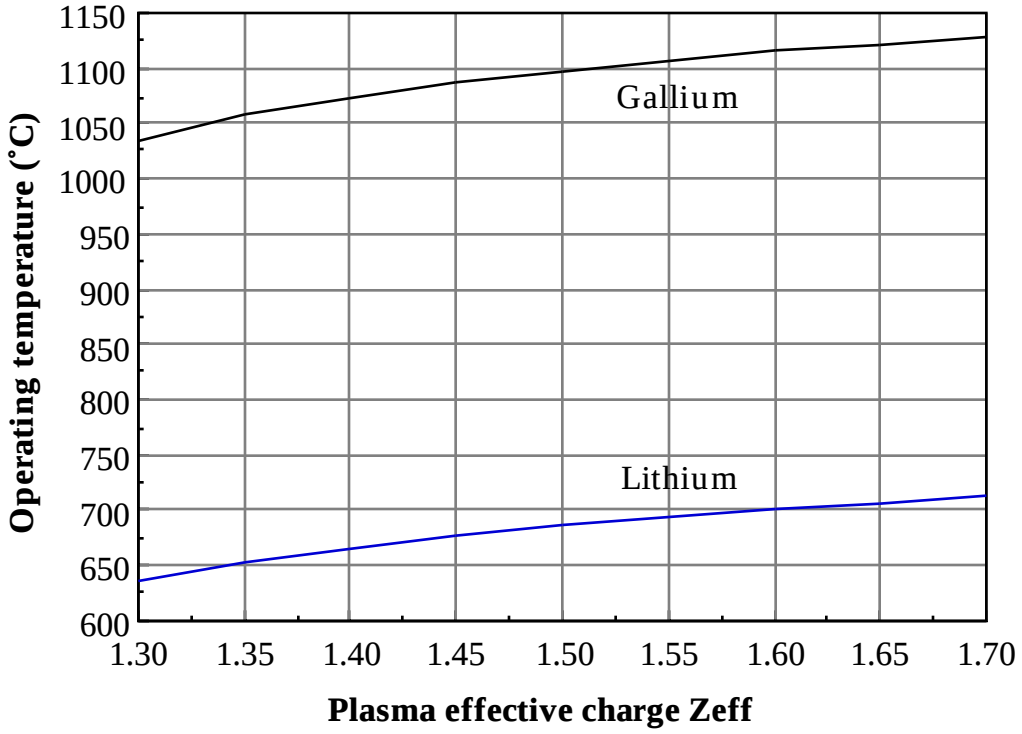

Fig. 2.7 Operating temperature *vs*. plasma effective charge Z_{eff} for ARIES-ST parameters. The divertor plasma temperature is 10eV.

Contamination due to evaporated LM is represented by an increase of plasma effective charge. Comparison of Fig.2.7 with Fig.2.8 shows that an order of increase of the compression factor for lithium vapor does not increase too much the operation temperature range. If Z_{eff}=1.7 is the limit for the plasma effective charge state, an increase of 138.8˚C of the operating temperature is

achieved. From Figs. 2.7, 2.9 and 2.10, we can see that in order to keep the increase of plasma effective charge Z_{eff} within 0.1~0.5, the operating temperature for gallium is 1037.6~1130.9˚C, while for lithium it is 635.7~714.0˚C; the partial pressure of gallium vapor at divertor is 8.56×10^{-3} Torr ~ 4.28×10^{-2} Torr while for lithium it is 0.133~0.663 Torr; the ratio of Ga-ion density to the electron density at the plasma core is 1.1×10^{-4}~5.4×10^{-4} while it is 1.67~8.33% for lithium; the normal handling capacity of the divertor heat flux is 33.0~36.0 MW/m^2 for gallium while it is 25.0~29.3 MW/m^2 for lithium. All these results are obtained when the plasma temperature is assumed to be 10 eV. From Fig.2.13 we can see that requirement of low plasma temperature at the divertor does not reduce much the handling capacity of divertor heat flux by the LM surface. For instance, when Z_{eff} =1.7 is maintained, decreasing the plasma temperature at the divertor from 10 to 5 eV (at which in most cases the plasma has been detached) can only reduce the handling capacity for gallium from 36.0 MW/m^2 to 34.7 MW/m^2 and reduce the handling capacity for lithium from 29.3 MW/m^2 to 27.4 MW/m^2.

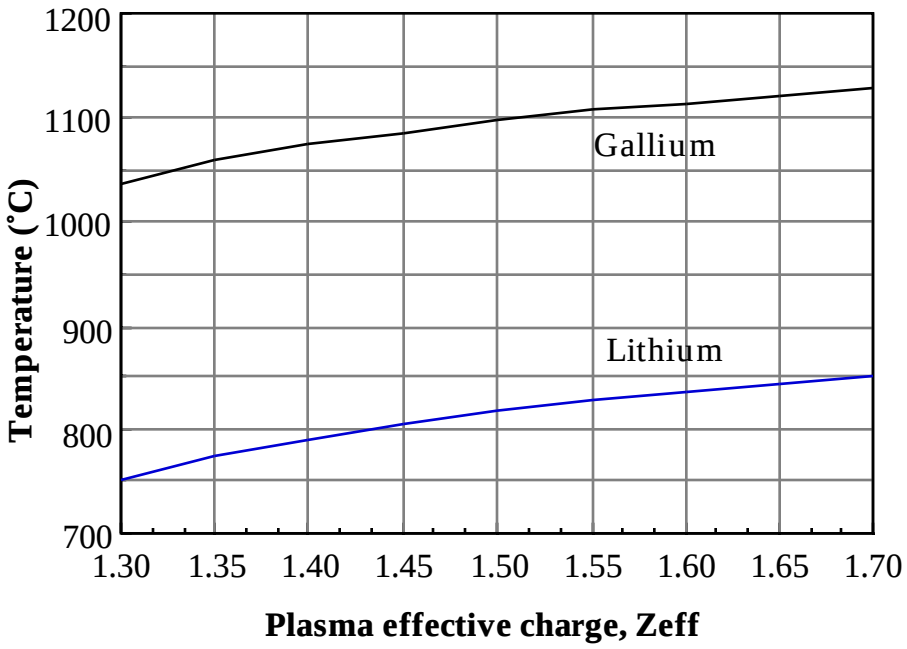

Fig. 2.8 As in Fig.2.7 but compression ratio for lithium vapor is 20.0, the same as gallium, instead of 2.0.

Table 2.3 corresponds to Table 2.2 but is based on the second method and the parameters of ARIES-ST from which we can see the operation parameters for LM divertor. The case for different compression ratios for lithium vapor corresponding Z_{eff} =1.7 is shown in Table 2.4.

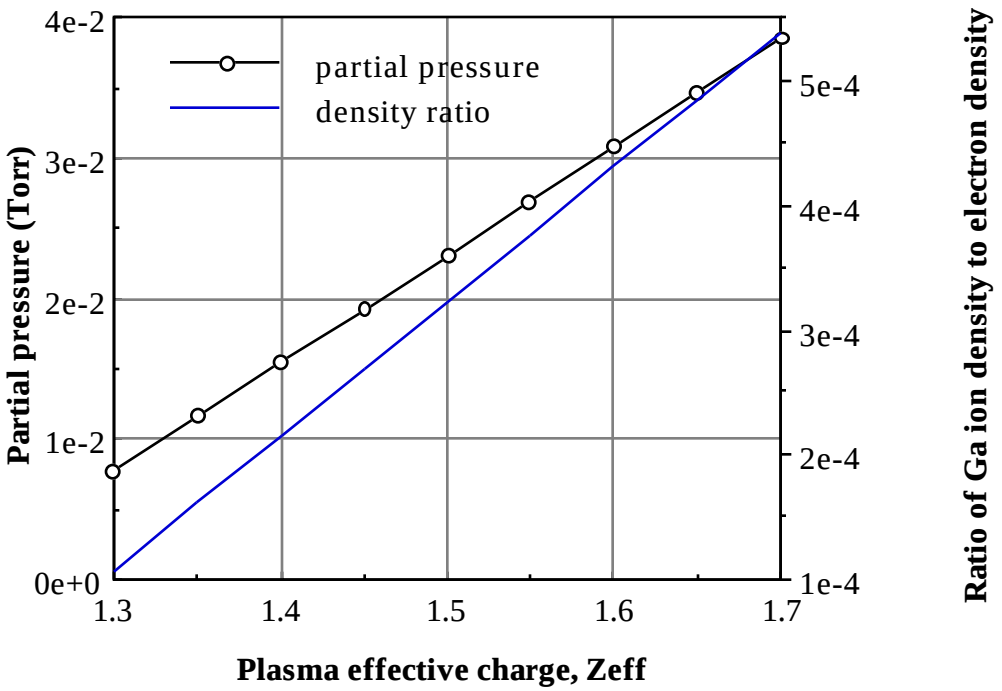

Fig. 2.9 The saturated gallium vapor pressure at divertor and gallium ion density as impurity in the plasma core versus the plasma effective charge Z_{eff}. The divertor plasma temperature is 10 eV.

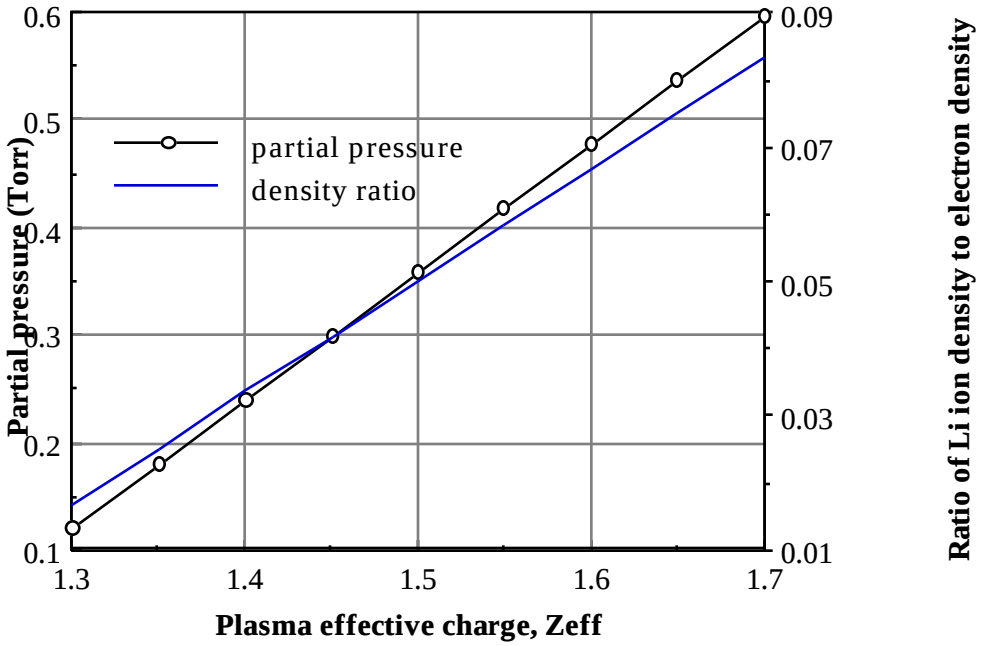

Fig. 2.10 The saturated lithium vapor pressure at divertor and lithium ion density as impurity in the plasma core versus the plasma effective charge Z_{eff} for the case that the compression ratio for lithium vapor at divertor is 2.0. The divertor plasma temperature is 10 eV.

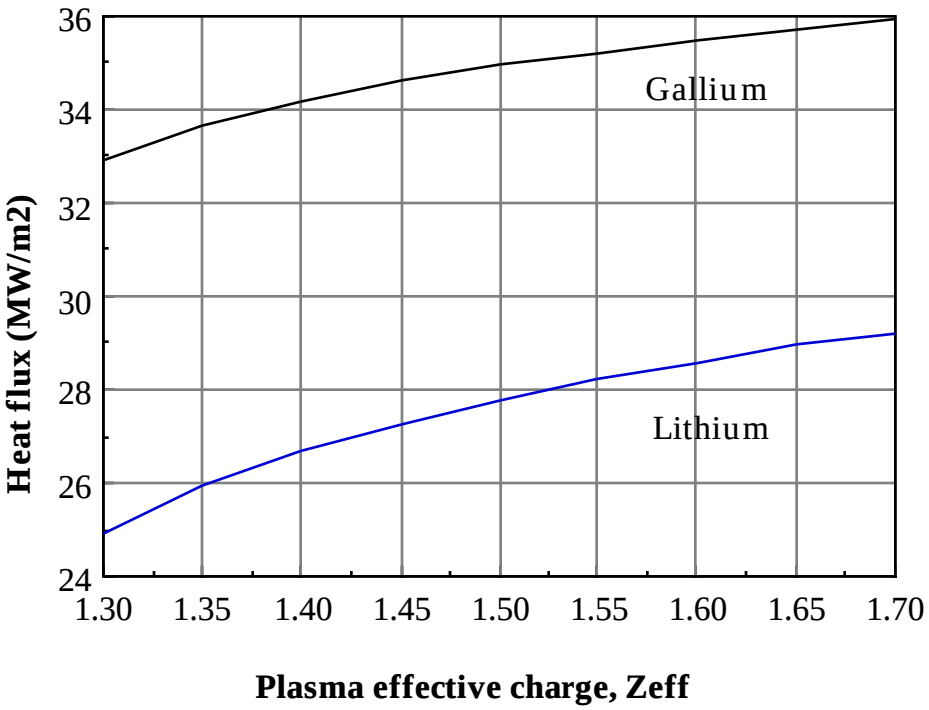

Fig. 2.11 The normal handling capacity of the divertor heat flux of gallium and lithium film divertors versus the plasma effective charge Z_{eff} for the case that the compression ratio for lithium vapor at divertor is 2.0. The divertor plasma temperature is 10eV.

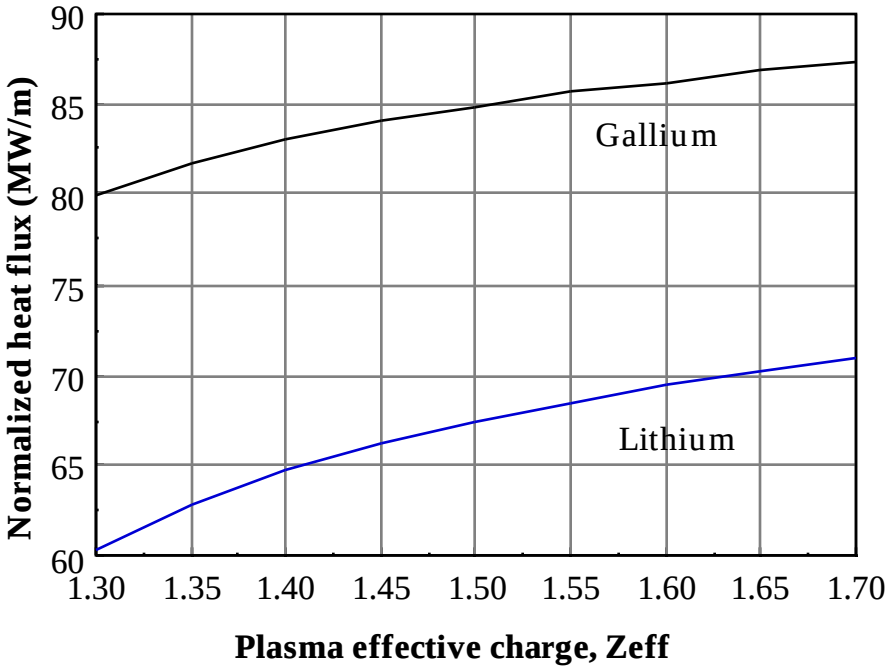

Fig. 2.12 The normal handling capacity of the normalized divertor heat flux of gallium and lithium film divertors versus the plasma effective charge Z_{eff} for the case that the compression ratio for lithium vapor at divertor is 2.0. The divertor plasma temperature is 10 eV.

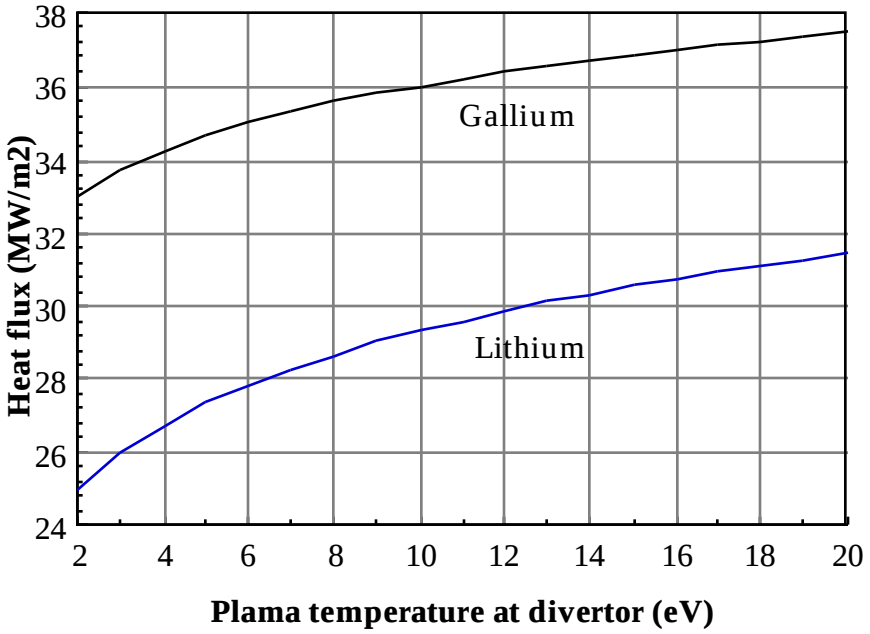

Fig. 2.13 The normal handling capacity of the divertor heat flux of gallium and lithium film divertors versus the plasma temperature T_{div} for the case that the compression ratio for lithium vapor at divertor is 2.0 and Z_{eff}=1.7.

Table 2.3 Estimate of handling capacity of heat flux by use of compression factor method

Compression factors at divertor	Gallium		20.0
	Lithium		2.0
Plasma parameters	Electron density n_e		$3.03\times10^{20}/m^3$
	Ion temperature T_i		11.66 keV
	Z_{eff}		1.3–1.4
Increase of Z_{eff} due to LM vapor	ΔZ_{efff}		0.1–0.2
Working temperature window	Gallium	ΔZ_{efff}=0.1	(29.8–1037.6)°C
		ΔZ_{efff}=0.2	(29.8–1076.2)°C
	Lithium	ΔZ_{efff}=0.1	(186–635.7)°C
		ΔZ_{efff}=0.2	(186–667.8)°C
Normal handling capacity of divertor	Ga-film		(32.97–34.24) MW/m^2
	Ga-drop		(13.54–14.07) MW/m^2
	Li-film		(24.97–26.76) MW/m^2
	Li-drop		(6.29–6.74) MW/m^2
Saturated vapor pressure	Gallium		$(0.8–1.6)\times10^{-2}$ Torr
	Lithium		(0.12–0.25) Torr
Impurity concentration in plasma core n_{LM}/n_e	Gallium		$(1.075-2.151)\times10^{-2}$%
	Lithium		1.667% –3.333%

Table 2.4 Typical divertor parameters of LM divertor for ARIES-ST (Z_{eff}=1.7)

Average ion temperature (keV)	11.66	11.66
Average electron density (m^{-3})	3.029×10^{20}	3.029×10^{20}
divertor plasma temperature (eV)	10	10
Compression ratio for gallium vapor	20.0	20.0
Compression ratio for lithium vapor	2.0	20.0
$C_Z^{P,ave}$ for gallium	1.69×10^{-2}	1.69×10^{-2}
$C_Z^{P,ave}$ for lithium	1.69×10^{-2}	1.69×10^{-3}
Plasma effective charge Z_{eff}	1.7	1.7
Operation temperature of gallium divertor (°C)	1128.9	1128.9
Saturated vapor pressure of gallium at divertor (Torr)	3.85×10^{-2}	3.85×10^{-2}
Ratio of Ga ion density to electron density in core	5.38×10^{-4}	5.38×10^{-4}
Operation temperature of lithium divertor (°C)	712.3	851.1
Saturated vapor pressure of lithium at divertor (Torr)	0.597	5.969
Ratio of Li ion density to electron density in core	8.33×10^{-2}	8.33×10^{-2}

3. LIQUID METAL DROPLET CURTAIN DIVERTOR

For a liquid-metal droplet curtain divertor, the maximum size of the droplet is determined by the LM surface tension that is a function of the temperature. The surface tension σ_s^{ga} (N/m) for gallium is [26]:

$$\sigma_s^{ga} = 0.718 - 1.01\times10^{-4}(T - T_m) \tag{3.1}$$

The radius of a droplet of gallium is obtained based on equilibrium of pressure due to surface tension with that caused by gravity of the LM drop:

$$R=\sqrt{\frac{3\sigma_s^{ga}}{2\rho g}} \tag{3.2}$$

We assume that the droplet rotates rapidly or receives uniform heat flux from all directions when it drops down so that all the surface of a droplet is exposed to the plasma heat flux. In this case, the radial distribution of temperature of the sphere is governed by:

$$\frac{\partial^2 T(r,t)}{\partial r^2} + \frac{2}{r}\frac{\partial T(r,t)}{\partial r} = \frac{1}{\alpha}\frac{\partial T}{\partial t} \tag{3.3}$$

The boundary conditions at the surface of the droplet (r=R) are:

(i) T=T_0 at t=0
(ii) $\partial T / \partial r\big|_{r=R} = -\Gamma / \kappa$

The handling capacity of heat flux determined this way underestimates the actual value in the reactor case in which the droplet is irradiated from only one direction. If the handling capacity of heat flux is underestimated by a factor q_{en}, it should satisfy:

$$1 < q_{en} \le \frac{\Gamma\ 4\pi r^2}{\iint \vec{\Gamma} \cdot d\vec{S}} \tag{3.4}$$

In the case of a LM droplet divertor, the heat flux dumps parallelly onto the front hemisphere of the droplet which is treated approximately as a sphere. The beneficial effects coming from the tilting of the surface divertor concepts do not exist for the droplet concepts because of symmetry of the sphere itself. For simplicity but losing no generality, let's suppose that the heat flux is along z axis, then:

$$\begin{aligned} \iint \vec{\Gamma} \cdot d &= \Gamma \iint \vec{e_z} \cdot \vec{e_r}\ dS \\ &= \Gamma \int_{\pi/2}^{0} \int_{2\pi}^{0} r^2 \sin\theta\ \cos\theta\ d\theta\ d\phi \\ &= \Gamma\ \pi\ r^2 \end{aligned} \tag{3.5}$$

Therefore the underestimated factor due to rotation or exposure in all direction is less than or equal to 4 in the case of tokamak divertor. The solution of Eq.(3.3) for $t \le \tau$, the duration of the droplet exposed to the plasma heat flux, is:

$$T(r,t) = T_0 + \frac{\Gamma R^2}{r\kappa}\left[-e^{-\frac{R-r}{R}} e^{\frac{\alpha t}{R^2}} erfc\left(-\frac{\sqrt{\alpha t}}{R} + \frac{R-r}{2\sqrt{\alpha t}}\right) + erfc\left(\frac{R-r}{2\sqrt{\alpha t}}\right)\right] \tag{3.6}$$

where R is the radius of the droplet. At the surface of the droplet, the variation of the temperature with time is:

$$T(R,t) = T_0 + \frac{\Gamma R}{\kappa}\left[-e^{\frac{\alpha t}{R^2}} erfc\left(-\frac{\sqrt{\alpha t}}{R}\right) + 1\right] \tag{3.7}$$

from which we can see that the increase of temperature at the surface of the droplet increases exponentially with time. This is quite different from the case of the film flow in which the increase of the temperature of the film surface is much slower with time. When the underestimate factor due to the assumption of uniform exposure of the sphere surface is taken into account, the handling capacity of heat flux by a droplet is:

$$\Gamma = \frac{q_{en}\kappa\left(T_{op}-T_m\right)}{R}\left[e^{\frac{\alpha\tau}{R^2}}erfc\left(\frac{\sqrt{\alpha\tau}}{R}\right)+1\right]^{-1} \tag{3.8}$$

where T_{op} is the operation temperature of LM. Inserting Eq.(2.11) and Eq.(3.2) into Eq.(3.8), the divertor heat flux the droplet curtain can handle takes the form:

$$\Gamma = q_{en}\kappa\left(T_{op}-T_m\right)\sqrt{\frac{2\rho g}{3\sigma_s}}\left[\exp\left(\frac{2\rho g\alpha Q\lambda_{mp}}{3\sigma_s v_{av}\sin\eta}\right)erfc\left(\sqrt{\frac{2\rho g\alpha Q\lambda_{mp}}{3\sigma_s v_{av}\sin\eta}}\right)+1\right]^{-1} \tag{3.9}$$

3.1 Heat flux handling capacity of LM droplet curtain divertor by constant liquid metal partial pressure method

Based on this method, the operation temperature of the LM divertor for the droplet case, which is determined by Eq.(2.18) is the same as in the film case which is shown in Fig.2.4. The handling capacity of divertor heat flux of LM droplet curtain divertor obtained from Eq.(2.18) and Eq.(3.9) for normal operation situation is shown in Fig.3.1. While the handling capacity of normalized heat flux is shown in Fig.3.2.

For the parameters shown in Table 2.1, the maximum handling capacity of divertor heat flux is 31.9 MW/m^2 for a gallium droplet curtain, while it is 16.6 MW/m^2 for lithium droplets.

The operating temperature window is the same as the film case for both gallium and lithium which is shown in Fig.2.4. When the increment of Z_{eff} due to LM vapor is 0.1–0.2, the normal handling capacity of divertor heat flux is 17.2–17.9 MW/m^2 for gallium and 12.2–13.2 MW/m^2 for lithium which is also given in Table 2.2 for comparison with film case. The corresponding handling capacity of normalized heat flux is 41.7–43.5 MW/m for gallium and 29.6–32.0 MW/m for lithium. Compared with film configuration of LM divertor (from Table 2.2), we can conclude that the handling capacity of divertor heat flux for the droplet curtain concept is quite limited by the size and configuration of the droplet itself.

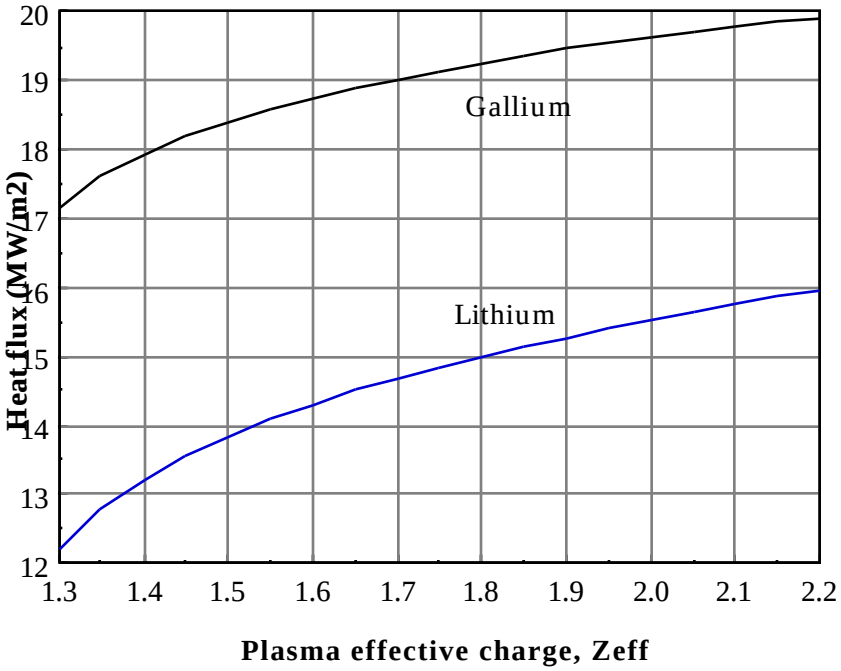

Fig. 3.1 The relationship of the normal handling capacity (MW/m^2) of divertor heat flux which the liquid gallium and lithium droplet curtain divertors can handle at normal conditions with the plasma effective charge Z_{eff} for typical fusion plant parameters shown in Table 2.1.

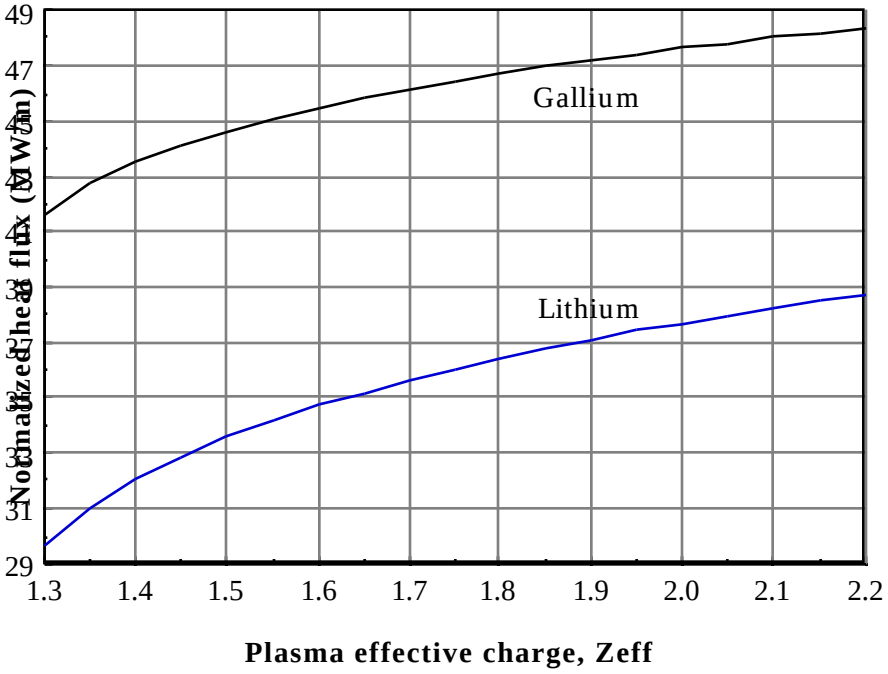

Fig. 3.2 The relationship of the normalized heat flux (MW/m) which the gallium and lithium droplet curtain divertors can handle at normal conditions with the plasma effective charge Z_{eff} for typical fusion plant parameters shown in Table 2.1.

3.2 Heat flux handling capacity of LM droplet curtain divertor by compression factor method

Modeling for this method and parameters used are the same as in Section 2.2b. In this section, compression factors of 20 for gallium and 2.0 for lithium are used. The operation temperature for the droplet configuration is also determined by Eq.(2.23), the same as the film case which is shown in Fig. 2.7. The saturated gallium (lithium) vapor pressure at divertor and gallium (lithium) ion density as impurity in the plasma core versus the plasma effective charge Z_{eff} is also the same as film case which are shown in Fig. 2.9 (Fig.2.10). The normal handling capacity of the divertor heat flux can be obtained from Eq.(3.8). The result versus the plasma effective charge Z_{eff} for the case that the compression ratio for lithium vapor at divertor is 2.0 is shown in Fig. 3.3. The corresponding handling capacity of the normalized divertor heat flux of LM droplet divertor is shown in Fig. 3.4. The normal handling capacity of the divertor heat flux of gallium and lithium droplet divertors versus the plasma temperature T_{div} at divertor when Z_{eff}=1.7 is shown in Fig.3.5.

From the above results we can see that to keep the increase of plasma effective charge Z_{eff} to be within 0.1~0.5, the normal handling capacity of the divertor heat flux is 13.6~14.8 MW/m^2 for gallium droplet configuration while it is 6.3~7.4 MW/m^2 for the lithium droplet case. All these results are obtained when the divertor plasma temperature is assumed to be 10 eV. From Fig.3.5 we can see that when Z_{eff} =1.7 is maintained, decreasing the plasma temperature at the divertor from 10 eV to 5 eV (at which in most cases the plasma has been detached from divertor surface) can only reduce the handling capacity for gallium droplet from 14.8 to 14.2 MW/m^2 and reduce the handling capacity for lithium droplet from 7.4 to 7.0 MW/m^2. Table 2.3 is the corresponding table of Table 2.2 but based on the second method and the parameters of ARIES-ST from which we can see the operation parameters for LM film divertor and droplet divertor.

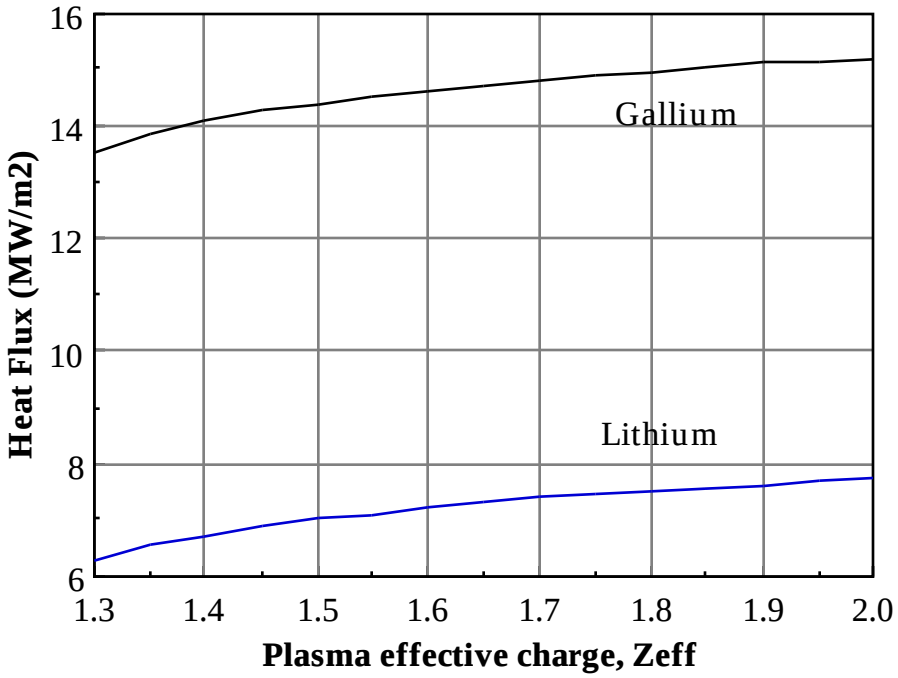

Fig. 3.3 The normal handling capacity of the divertor heat flux of gallium and lithium droplet curtain divertors versus the plasma effective charge Z_{eff} for the case that the compression ratio for lithium vapor at divertor is 2.0.

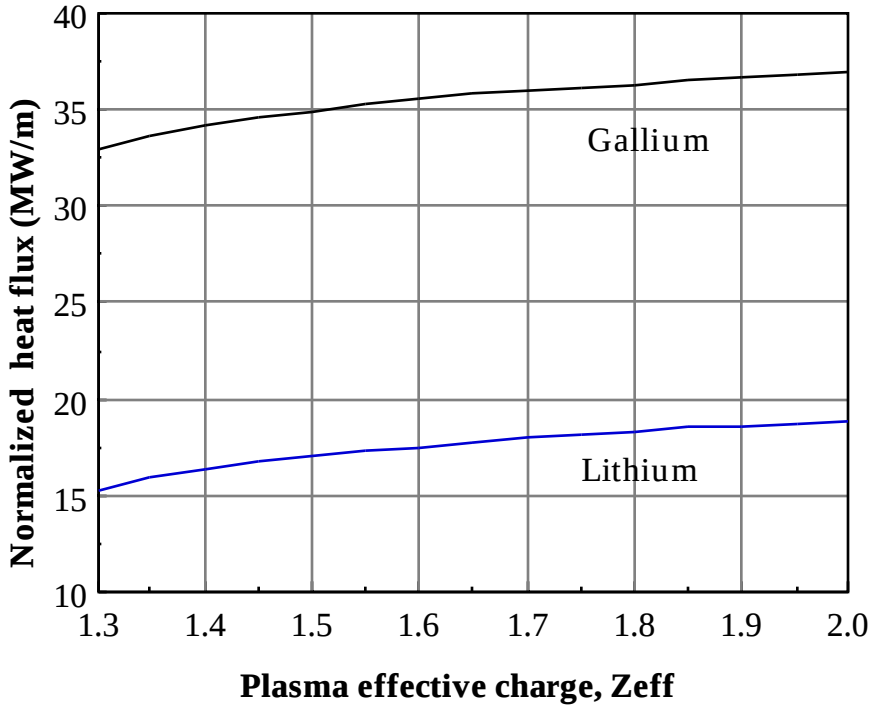

Fig.3.4 The handling capacity of the normalized divertor heat flux of gallium and lithium droplet curtain divertors versus the plasma effective charge Z_{eff} for the case that the compression ratio for lithium vapor at divertor is 2.0.

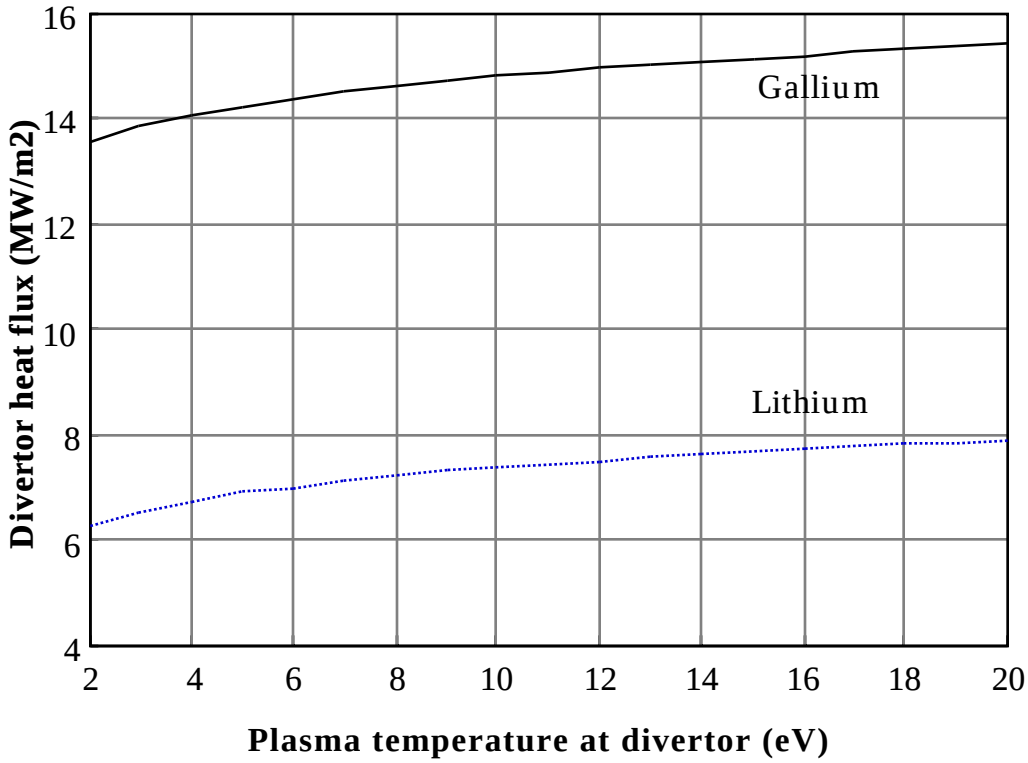

Fig. 3.5 The normal handling capacity of the normalized divertor heat flux of gallium and lithium film divertors versus the plasma temperature T_{div} for the case that the compression ratio for lithium vapor at divertor is 2.0.

4. THICKNESS OF FILM FOR THE FILM LM DIVERTOR

From the analyses in Sections 2 and 3 we can see that the film configuration is better than the droplet from the point of view of handling capacity of divertor heat flux. We have also discussed the film thickness from the point of the heat transfer. In this section we will discuss this issue further.

For a LM film divertor, it is important that the film be kept in a flat and homogeneous surface profile. However, the incidence of the plasma momentum flux is oblique in a tokamak reactor. Oblique incidence of the plasma wind in a chute of finite dimension tends to push the flat LM surface into a wave-like profile. The detrimental effect is that it's quite possible for the underlying solid surface (substrate) to be exposed to the plasma particles if the film is not thick enough. Therefore, film thick enough to protect the underlying surface is important for LM film divertor design. In this section we will determine what is the minimum thickness of the film to prevent exposure of the underlying solid surface directly to the plasma particles. Three different physical

situations are considered in the estimate of the thickness of the film. The first is from the penetration of the electromagnetic field; the second is from the physical sputtering process due to bubble formation of plasma particles; and the last is from the magnetohydrodynamic stability of the LM film.

4.1 Penetration depth into LM film of electromagnetic field

The LM film for the divertor is in a strong magnetic environment, it is a important process for the magnetic field to penetrate into the film. This process happens especially during the ramp-up of the plasma, shut-down, ELM, and disruptions. It is important in the estimation of the LM film thickness because of its magnetohydrodynamic properties [27] and the limited thickness of ~mm of the film [28,29]. Magnetic field is "freezed" in the liquid metal. "Adherence" of the liquid metal to the magnetic lines of force means that disturbances of magnetic lines of force will result in fluid-mechanical disturbances in the LM. Thus, the layer of the film with "freezing-in" of magnetic lines of force is not reliable. Supposing the length of the film exposed to the plasma is L, the thickness of the film is h, and the constant magnetic field is B_o, the propagation of magnetic field into the region just above the film is:

$$\frac{\partial B}{\partial t} = \frac{1}{\sigma\mu_0} \quad ^2 B \tag{4.1}$$

Here the penetration depth δ_o is defined as the decay length of the electromagnetic field at $B=B_o/e$. The solution of Eq.(4.1) is:

$$\frac{B}{B_0} = G(u) = \frac{2}{\sqrt{\pi}} \int_u^{\infty} e^{-u^2} du \tag{4.2}$$

with

$$u = \sqrt{\frac{\mu_0 \delta^2 \sigma}{4t_0}} \sqrt{\frac{t_0}{t}} \frac{x}{\delta_0} \tag{4.3}$$

t_o is the time of observation for the penetration process. It is taken as the duration of the transient processes such as start-up, shut-down of plasma, ELM, and disruptions.

At the time of penetration or observation, $\frac{B}{B_0} = \frac{1}{e}$, and Eq.(4.3) will be:

$$u = \sqrt{\frac{\mu_0 \delta^2 \sigma}{4t_0}} \tag{4.4}$$

Therefore, the penetration length into the LM film of the electromagnetic field is:

$$\delta_0 = G^{-1}(1/e)\sqrt{\frac{4t_0}{\mu_0 \sigma}} \tag{4.5}$$

where $G^{-1}(1/e)$ is the value of the inverse Gauss error function.

4.2 Estimate of the film thickness from bubble formation

Experiments of gallium sputtering on the test facility of the Moscow Physical Engineering Institute showed that the sputtering rate increases with the injected particle flux [30]. This result can be interpreted based on analogy with blistering [31]. Injected hydrogen is most likely absorbed by the LM film and bubbles are formed. Increase of the size of the bubbles results finally in explosion of the bubbles which is associated with sputtering of the liquid metal that will contaminate core plasma. The time from the formation to explosion of the bubble is important for the design of the film length and the speed at which the film flows. It is desirable that this time-period is greater than the exposing time of the LM film and thus the discharge of the content of the bubble and the associated sputtering can be controlled by using of a baffling structure (refer to Fig.4.1).

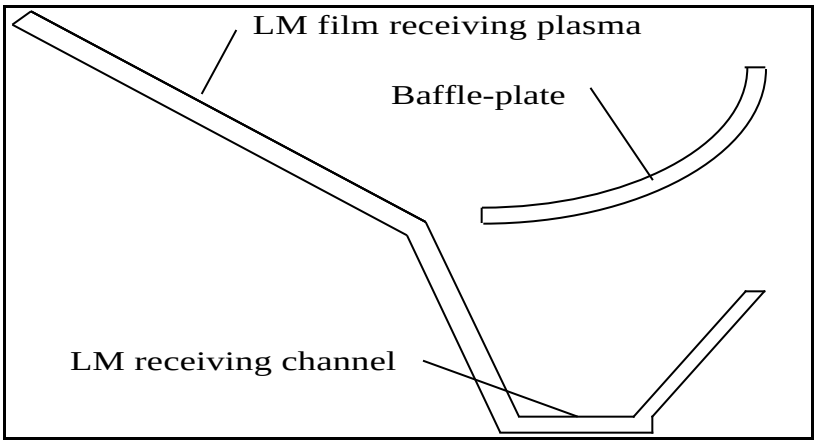

Fig.4.1 Demonstration of position of the baffle-plate relative to the LM film for divertor surface in a fusion reactor.

The balance of a bubble formed in the LM film is determined by all the forces exerting on it. The criteria for a bubble of size r not to float out of the film surface is that the forces acting downward on the bubble should not be smaller than those upward. This results in the following formula for the bubble size:

$$r \le r_c = \sqrt{\frac{3}{2}\frac{\sigma_s}{\rho g}} \tag{4.6}$$

where σ_S is the LM surface tension, ρ is the LM mass density and g is the gravitational acceleration. The growth of the bubble is estimated to be [32]:

$$r(t) = r_0 \exp(t/\tau_d) \tag{4.7}$$

with r_o~1 nm being the radius of the seeding bubble [33], $\tau_d = 16\sigma_s / 3kT\Gamma_i$ with Γ_i being the average plasma ion influx, kT is the plasma ion temperature. t should satisfy:

$$t \le t_{eff} = L_{eff} / v_{av} \tag{4.8}$$

where L_{eff} is the effective dimension of the plasma projecting on the film, and v_{av} is the average velocity at which the LM film flows through the plasma shadowing area. The time needed for the bubble to grow to the maximum size r_c is:

$$t_c = \tau_d \ln\frac{r_c}{r_0} = \frac{8\sigma_s}{3kT\Gamma_i} \ln\left(\frac{3}{2}\frac{\sigma_s}{\rho g r_0^2}\right) \tag{4.9}$$

The condition for bubbles not to erupt is $t_{eff} \le t_c$, *i.e.*

$$v_{av} \ge \frac{3kT\Gamma_i}{8\sigma_s}\left[\ln\left(\frac{3}{2}\frac{\sigma_s}{\rho g r_0^2}\right)\right]^{-1} L_{eff} \tag{4.10}$$

This is a very important expression for the safe design of the LM flow speed.

4.3 Sustainment of a stable and homogeneous LM film

A stable and homogeneous LM film is important for the feasibility of the LM divertor in a fusion reactor. Simulation using RIPPLE code in a certain range of edge plasma parameters demonstrated that a LM film of several millimeters can withstand the plasma wind, especially for gallium [28]. However, the code they used is a flow code not a magnetohydrodynamic one [34], the stability enhanced by magnetic field [35] is not taken into account. Experimental results [29] show that the

non-uniformity in the film thickness along the chute width decreases with increment of magnetic field which inclines the film surface. Surface waves can be suppressed by the magnetic field. Analysis of the LM film surface MHD instability from interaction of steady plasma flow with the LM film showed that both the magnetic field (perpendicular to the surface) and the plasma at the film surface are favorable in the instability suppression [35]. Supposing the LM film flows along the supporting chute which has an angle with the horizontal. When plasma wind effect is not taken into account, the film flow velocity v_0 and the film thickness h_0 of a homogeneous film in a coplanar magnetic field should satisfy [37]:

$$v_0 = \frac{g h_0^2 \sin\theta}{3\upsilon + \Lambda h_0^2} \tag{4.11}$$

where g is the acceleration due to gravity, υ is the kinematic viscosity, θ is the angle between and the bottom surface of the chute on which the film flows, Λ is given by $\Lambda = \frac{2B}{b}\sqrt{\frac{\sigma\upsilon}{\rho}}$ where B is the magnetic field, b is the width of the chute, σ and ρ are the conductivity and mass density of the film respectively. The relationship between the velocity at which the film flows and the thickness of the film when θ=30˚ is shown in Fig.4.2. Fig.4.2a is for different magnetic field when the width of the chute b=0.5 m and Fig.3b is for different width of the chute when the magnetic field is B=5 Tesla. The limit case for heat transfer in which the thickness is 12.5 mm for gallium is also shown in Fig.4.2b from which we can see that the velocity required is no more than 5 m/s. These results are for the case that the wall of the chute is non-conducting. For the case that the wall of the chute is conducting, these exists a thickness interval in which these will be no steady-state film flow for a certain range of parameters of magnetic field and wall conductivity [37]. This should be avoided in the LM film divertor concept.

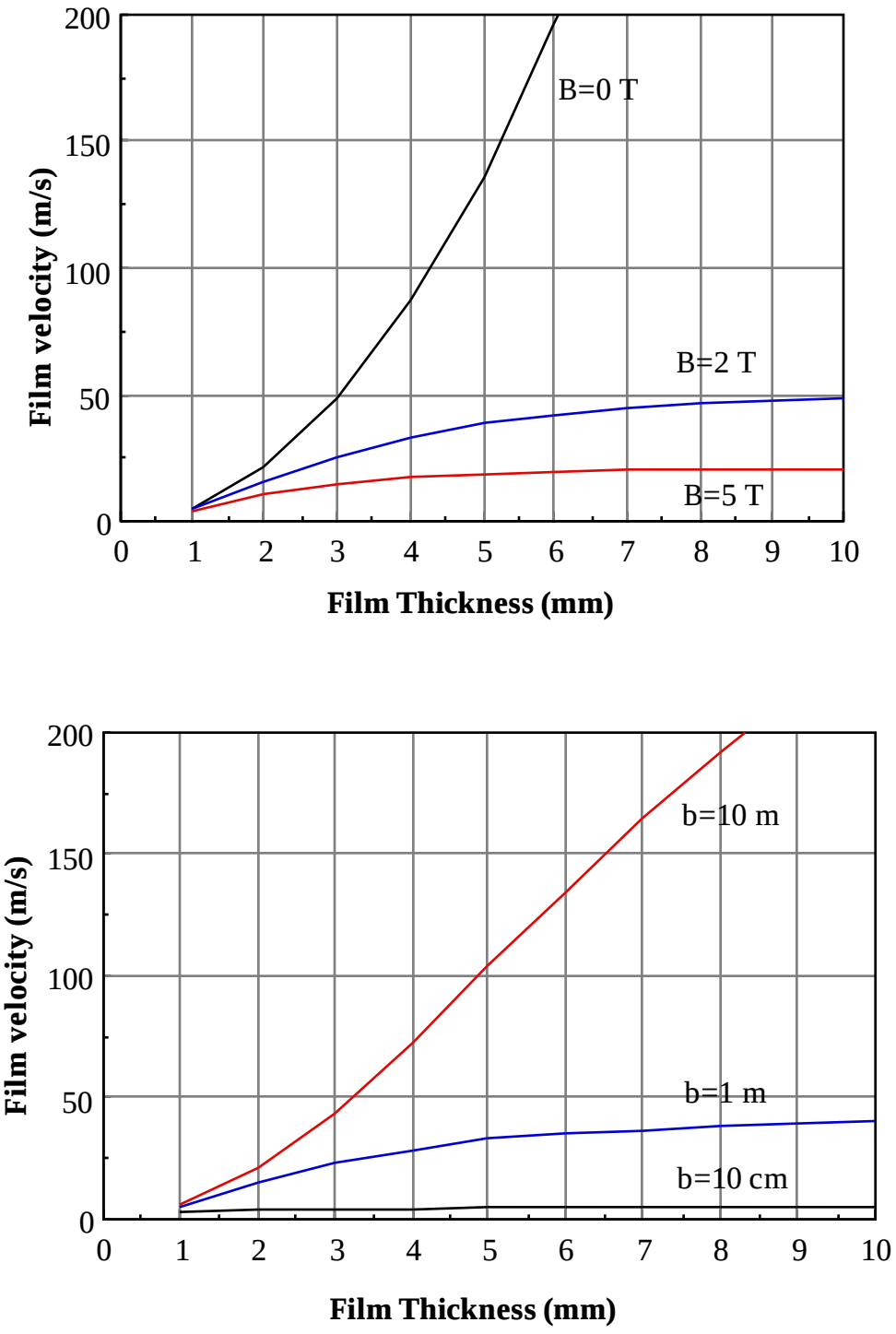

Fig.4.2 Relationship between the velocity at which the film flows and the film thickness when θ=30°. (a) For different magnetic field while b=0.5m; and (b) For different chute width b while B=5 T.

5. DIVERTOR SPACE AND TOTAL RADIATION ASSOCIATED WITH LM DIVERTOR OPERATION

5.1 Compact LM divertor space

Helium exhaust is one of the major concerns when liquid metal is used as a divertor surface. The production rate of helium in a fusion reactor whose fusion power is P_f(MW) is $\Gamma_{He}=3.57\times10^{17}P_f$ (s^{-1}). The confinement time of helium is defined as:

$$\begin{aligned}\tau^{*}_{He} &= \langle n_{He}\rangle V^{main}/\Gamma_{He} \\ &= f_{he}\langle n_e\rangle V^{main}/\Gamma_{He}\end{aligned} \tag{5.1}$$

where f_{He} is the constant concentration of helium in the plasma core, $<n_e>$ is the average electron density in the plasma core, and V^{main} is the volume of core plasma. Using a simple two-chamber model [25] where the divertor chamber and main chamber are treated as different in the helium concentration due to enrichment in the divertor chambers, the effective pumping speed S_{eff} in a fusion reactor with double-null configuration should be determined by:

$$S_{eff} = \frac{1}{\tau^{*}_{He}}\left(2V^{div} + \frac{V^{main}}{C_{He}}\right) \tag{5.2}$$

where V^{div} is the volume of one of the two divertor chambers in ARIES-ST, C_{He} is the compression factor for helium, which is define as $C_{He} = n^{div}_{He}/n^{core\ edge}_{He}$ with $n^{core\ edge}_{He}$ being helium density at the edge of the core plasma, usually evaluated at normalized minor radius ρ=0.7 for ELMy H-mode operation plasma [23]. The above expression is obtained based on the fact that helium, generated in a D-T burning plasma and after certain concentration is reached, must be removed at exactly the same rate as produced to avert extinguishment of plasma due to its accumulation. From Eq.(5.1) and (5.2), we can obtain the volume of divertor chamber necessary for helium pumping:

$$V^{div} = \frac{V^{main}}{2}\left(\frac{S_{eff} f_{He}\langle n_e\rangle}{\Gamma_{He}} - \frac{1}{\eta_{He}C_{D2}}\right) \tag{5.3}$$

where $C_{D_2} = 2n^{div}_{D_2}/n^{core\ edge}_{e}$ is the compression factor for hydrogen isotopes. A value of 6 is attainable in present tokamak experiments [25]. η_{He} is the He enrichment factor [38,25] in the divertor region. Usually the value of η_{He} is from 0.2 to 0.5. Typical parameters are given in Table 5.1 for ARIES-ST, where the divertor chamber space needed for helium exhaust is given for two cases of effective pumping speed.

Table 5.1 Parameters for divertor space and helium pumping requirements

Main plasma volume (m^3)	509.816	509.816
α particle concentration in core plasma	10%	10%
α particle production rate (1/s)	1.25×10^{21}	1.25×10^{21}
α particle confinement time (s)	12.41	12.41
He enrichment factor η_{He}	0.2	0.2
Compression factor of hydrogen isotopes C_{D_2}	6.0	6.0
Effective pumping speed S_{eff} (m^3/s)	50	46
Volume of one of the two divertor chambers (m^3)	55.21	30.40

5.2 Radiation associated with LM divertor

In the following we will estimate the possible radiation associated with LM divertor. The impurity species associated with radiation is assumed to be the evaporated liquid metal.

Extrapolation of the radiative divertor regions observed in present experiments [39] to a future fusion reactor is accepted as a method to solve the erosion problem of the divertor due to high heat flux [40]. With the use of liquid metal (LM) as the plasma-contact surface, the requirements of low heat flux (≤5 MW/m^2) and thus detached or semi-detached plasma operation may not be so serious for tokamak reactor though the radiative plasma operation is still necessary to reduce the normalized divertor heat flux for very competitive power plant in which case the normalized divertor heat flux can be even greater than the handling capacity of the LM [41]. Supposing the burning plasma in the ARIES-ST is D-T with 10% Helium, the Z_{eff} of the plasma with the power radiated can be estimated from the scaling radiative plasma law [42]:

$$Z_{eff} = 1.2 + \frac{5.6(\pm 0.7) P_{rad} Z^{0.19\pm0.05}}{S^{1.03\pm0.2}\,\bar{n}_e^{\,1.95\pm0.04}} \tag{5.4}$$

where P_{rad} is the total power radiated (in MW), S is the main plasma surface area (m^2), $\bar{n}_e$ is the line averaged density in units of $10^{20}m^{-3}$, Z is the atomic number of the impurity. For a tokamak reactor, the total radiative plasma surface S is determined by [43]:

$$S = 4\pi^2 R_T a\left(1 - \frac{0.233\delta}{A}\right)\left[\frac{1+\kappa^2\left(1+2\delta^2-1.2\delta^3\right)}{2}\right]^{0.5} \tag{5.5}$$

where $A=R_T/a$ is plasma aspect ratio, δ is the plasma triangurality and κ is the plasma vertical elongation at the x-point. For ARIES-ST, R_T=2.93 m, a=1.83 m, A=1.60, δ=0.59, and κ=3.443, the total plasma surface is S=583.06m^2 (536.78 m^2 without triangularity correction). Although this is a preliminary scaling law based on the present experiment results, it can provide a good guide for the performance of radiative plasma edge operation associated with impurity. From Eq.(5.4), we can obtain the fraction of radiated power due to impurity:

$$f_{rad} = \frac{\left(Z_{eff} - 1.2\right) S^{1.03\pm0.2}\, \bar{n}_e^{1.95\pm0.04}}{5.6(\pm0.7)\, Z^{0.19\pm0.05} P_\alpha} \tag{5.6}$$

where P_α is the power of α particles. Supposing the radiated power is mainly due to the LM sputtered and evaporated at the divertor, then for ARIES-ST (P_α=532.67MW, R_t = 2.93 m, a=1.83 m, A=1.60, δ=0.59, κ_x=3.443, κ_{95}=3.200, $\bar{n}_e = 3.03\times10^{20}/m^3$, Z_{eff}=1.7), the fraction is f_{rad}=0.535 for gallium and 0.834 for lithium. This is obtained from Eq.(5.2) for the calculation of the plasma surface. However, the plasma shape factor is more represented by the flowing formula the plasma is highly triangularly twisted (δ_x>0.5) [43]:

$$S = 4\pi^2 R_T a\left(1 - \frac{0.233\delta}{A}\right)\left(\frac{1+\kappa_{95}^2}{2}\right)^{0.5} \tag{5.7}$$

It is 439 m^2 for ARIES-ST. Then, the fraction is f_{rad}=0.418 for gallium and 0.651 for lithium. These results are obtained based on the assumption that the contribution to Z_{eff} comes only from the impurity of the liquid metal from the LM divertor. The more detailed relation between the radiation fraction and the Z_{eff} is shown in Fig.5.1 which is based on the ARIES-ST parameters.

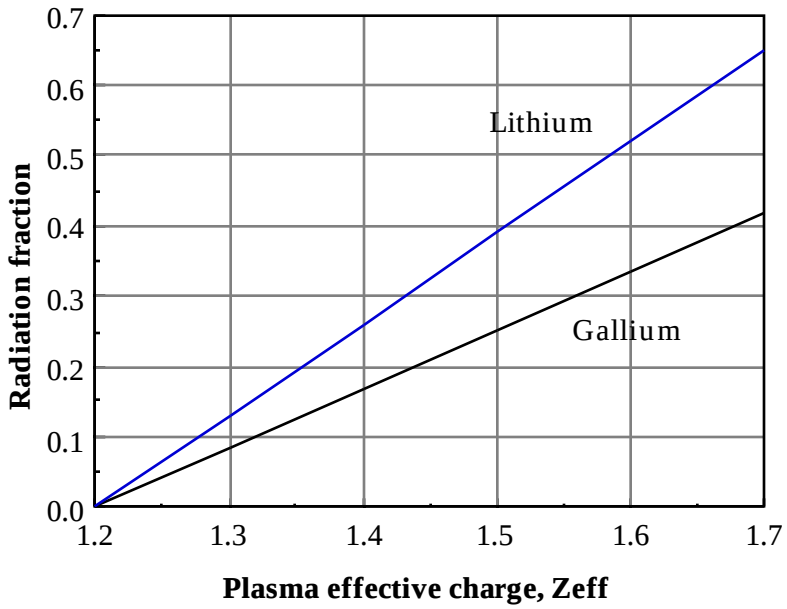

Fig. 5.1 The relation between the radiation fraction due to impurity of gallium and lithium divertor and the plasma effective charge.

6. DISCUSSION AND CONCLUSIONS

In the present report, the handling capacity of divertor heat flux by a LM divertor surface is estimated based on two methods, *i.e.*: i) constant LM impurity partial pressure from plasma core to divertor; ii) compression factor obtainable experimentally. To obtain the divertor heat flux capacity of a LM surface, the operating temperature of the surface is determined. The operating temperature in turn is determined by the tolerance of impurities (characterized by the plasma effective charge Z_{eff}) by the core plasma. The above-mentioned methods are used to determine the correlation between Z_{eff} and the operating temperature of LM surface divertor. Two different configurations of LM divertor are considered: film divertor and droplet curtain divertor. The results shown below represent heat flux limits with an increment of plasma effective charge due to LM impurity from 0.1 to 0.5.

Heat Flux Limits (MW/m^2)

	constant pressure	compression factor method
Ga Film	41.8–46.3	33.0–36.0
Ga Droplet	17.2–19.0	13.6–14.8
Li Film	48.5–58.3	25.0–29.3
Li Droplet	12.2–14.7	6.3–7.4

It can be readily seen that the results from the first method are higher than those obtained from the second method. This is because the corresponding temperature range from the first method is higher than the second. The operational temperature for gallium divertor (for both configurations) is from 1306.60 to 1444.63˚C (corresponding to ΔZ_{eff}=0.1 to 0.5) while it is 1037.60 to 1130.91˚C from the second method. As the second method is based on the present tokamak experiments, it should be more reasonable. Thus the first method may over-estimate the handling capacity of divertor heat flux. We conclude that the handling capacity of divertor heat flux of more than 20MW/m^2 is attainable for lithium film divertor, more than 30 MW/m^2 for gallium film divertor.

From the analyses above we can see that the moving belt can handle the largest divertor heat flux. For the moving belt concept the problem of heat transfer is transferred to the cooling of the moving belt. The other engineering problems such as neutron-induced thermal conductivity degradation of target plate material, tritium inventory, damage of the surface by neutrons and runaway electrons, fatigue life, reliability of the joining of the plasma-facing tiles with heat sink material at the roller, *etc.* encountered in the design of the solid surface divertor are almost the same as in the design of the moving belt divertor. All these problems should be solved before it is really established as the most robust divertor option.

Comparison of LM film divertor with droplet curtain divertor option show that the handling capacity of LM droplet is much smaller than that of film case.

We conclude that the handling capacity of divertor heat flux of more than 20 MW/m^2 is attainable for lithium film divertor, more than 30 MW/m^2 for gallium film divertor. The handling capacity of LM droplet curtain is quite limited by its size of the droplet and its intrinsic configuration. To make full use of the LM properties, LM film divertor seems to be preferable. Both gallium and lithium are capable to be used as the plasma-facing material from the present estimation. Anyway, trade-off studies of a plethora of other aspects must be accomplished before a final selection is made.

REFERENCES

[1] R. W. Conn, F. Najmabadi, and M. S. Tillack, "Prospects and issues for commercial fusion power systems", Presented at the 4th International Symposium on Fusion Nuclear Technology (ISFNT-4), April, 1997, Tokyo.

[2] F. Najmabadi, and the ARIES Team, "Overview of ARIES-RS Tokamak Fusion Power Plant", *ibid.*

[3] M. S. Tillack and the ARIES Team, "Engineering Design of the ARIES-RS Power Plant", *ibid.*

[4] ITER interim Report, 1996.

[5] D. L. Sevier, C. B. Baxi, D. N. Hill, E. E. Reis, G. W. Silke, C. P. C. Wong, Fusion Technology, **30** (1996) 720.

[6] S.V.Mirnov, V.N.Dem'yanenko, E.V.Murav'ev, J. Nucl. Mater., **196-198** (1992) 45.

[7] L.L.Snead and R.A.Vesey, Fusion Technology, **24** (1993) 83.

Y. Hirooka, M. S. Tillack, and A. Grossman, "Steady-State Impurity Control, Heat Removal and Tritium Recovery by Moving-Belt Plasma-Facing Components," 17th IEEE/NPSS Symposium on Fusion Engineering, San Diego, CA, Oct. 1997.

[8] N. C. Christofilos, J. Fusion Energy **8** (1989)97.

[9] B. Badger et al., Univ. of Wisconsin, Report UWFDM-68 VI. VII(1974).

[10] A. A. Abagyan *et al.*, At. Energ. **58** (1985) 252.

[11] S. V. Mirnov, V. N. Dem'yanenko, E. V. Murav'ev, J. Nucl. Mater. **196-198** (1992) 45.

[12] V. O. Vodyanyuk *et al.*, in: Questions of Atomic Science and Engineering, Series on Thermonuclear Fusion, **Vol.3** (1991) p.50.

[13] C. P. Liao, M. S. Kazimi, and J. E. Meyer, Fusion Technology, **23** (1993) 208.

[14] J. Laszlo and W. Eckstein, J. Nucl.Mater. **184** (1991) 22.

[15] C. P. Liao, M. S. Kazimi, Fusion Technology, **21** (1992) 1845.

[16] N. B. Morley and M. A. Abdou, Fusion Techno. **31** (1997) 135.

[17] C. S. Pitcher, A. W. Carlson, C. Fuchs, A. Herrmann, W. Suttrop, J. Schweinzer, M. Weinlich, ASDEX Upgrade Team, NBI Group, "Routes to Divertor Detachment in ASDEX Upgrade", J. Nucl. Mater. 241-243 (1997)696-700.

[18] R. B. Mohanti, J. G. Gilligan and M. A. Bourham, Fusion Technology, **30** (1996) 289.

[19] T. Kammash, Fusion Reactor Physics, Ann Arbor Science, 1975, p.391.

[20] C. P. C.Wong, E. Chin, T. W. Petrie, E. E. Reis, M. Tillack, X. Wang, I. Sviatoslavsky, S. Malang, D. K. Sze, "ARIES-RS Divertor System Selection and Analysis", to be published in Fusion Engineering and Design.

[21] G. Telesca, H. A. Claassen, P. Franz, A. M. Messiaen, J. Ongena, J. Rapp, U. Samm, N. Schoon, B. Schweer, M. Z. Tokar, B. Unterberg, G. Van Oost, J. Nucl. Mater. 241-243 (1997) 853.

[22] A. N. Nesmeyanov, R. Gary, Vapor pressure of the chemical elements, Elsevier Publishing Company, Amsterdam, 1963, p.423.

[23] M. J. Schaffer, M. R. Wade, R. Maingi, P. Monier-Garbet, W. P. West, D. G. Whyte, R. D. Wood, M. A. Mahdavi, "Divertor measurement of divertor exhaust neon enrichment in DIII-D", J. Nucl. Mater. 241-243(1997)585-589.

[24] J. K. Ehrenberg *et al*., J. Nucl. Mater., **241-243** (1997) 420.

[25] H.-S. Bosch, D. Coster, R.Dux, C. Fuchs, G. Haas, A. Herrmann, S.Hirsch, A. Kallenbach, J. Neuhauser, Z. R. Schneider, J. Schweinzer, M. Weinlich, ASDEX Upgrade team, NBI team, "Particle exhaust in radiative divertor experiments", J. Nucl. Mater. 241-243 (1997) 82-91.

[26] A. A. Karashaev, S. N. Zadumkin and A. I. Kukhno, Zh. Fiz. Khim., **41**(1967)654. English translation in: Russian Journal of Physical Chemistry, **41** (3) (1967) 329-330.

[27] Structure and properties of liquid metals.

[28] N. B. Morley, A. A. Gaizer, M. A. Abdou, "Estimates of the effect of a plasma momentum flux on the free surface of a thin film of liquid metal", Fusion Engineering and Design **28** (1995) 176-180.

[29] V. V. Baranov, I. A. Evtushchenko, I. R. Kirillov, E. V. Firsova, and V. V. Yakovlev, "Liquid metal film flow for fusion application", Magnetohydrodynamics, **30** (4) (1994) 553-560.

[30] L. B. Begrambekov, *et al*., At. Energ. 64 (1988) 212.

[31] S. V. Mirnov, V. N. Dem'yanenko, E. V. Murav'ev, "Liquid-metal tokamak divertors", J. Nucl. Mater. 196-198 (1992) 45-49.

[32] C. Liao, M. S. Kazimi and J. E. Meyer, "On hydrogen transport and edge plasma modeling of liquid-metal divertors", Fusion Technology **23** (1993) 208-217.

[33] L. B. Begrambekov, *et al.*, "Emission of material from the surface of a liquid metal under irradiation in a plasma", Magnetohydrodynamics, **23** (1987) 263.

[34] D. B. Kothe, R. C. Mjolsness and M. D. Torey, "RIPPLE: a computer program for incompressible flows with free surfaces," Technical Report LA-12007-MS, April 1991 (Los Alamos National Laboratory, Los Alamos, NM).

[35] V. A. Bernshtam, E. V. Poklonskii, and V. L. Sizonenko, "Surface stability in a hot-plasma liquid-metal limiter", Magnetohydrodynamics, **23** (4) (1987) 37-40.

[36] T. N. Aitov and B. A. Dityatkin, “Undulating flow of a thin layer of a viscous electrically conducting fluid in a coplanar magnetic field”, Magnetohydrodynamics, 23 (4) (1987) 383-388.

[37] A. Ya. Shishko, “A theoretical investigation of steady-state film flows in a coplanar magnetic field”, Magnetohydrodynamics, **28** (2) (1992) 75-88.

[38] M. Shimada, M. Nagami, K. Ioki, S. Izumi, M.Maeno, H.Yokomizo, K.Shiya, H.Yoshida, A. Kitsunezaki, N. H. Brooks, C. L. Hsieh, J. S. deGrassie, “Helium ash exhaust with single-null poloidal divertor in Doublet III”, Phys.Rev.Lett.47, (1981) 796-799.

[39] C. S. Pitcher, A. W. Carlson, C. Fuchs, A. Herrmann, W. Suttrop, J. Schweinzer, M. Weinlich, ASDEX Upgrade Team, NBI Group, “Routes to divertor detachment in ASDEX Upgrade”, J. Nucl. Mater. 241-243 (1997)696-700.

[40] JET Team (G. F. Matthews), Plasma Phys. Control Fusion **37** (1995) A227.

[41] P. H. Rebut *et al*., Fusion Eng. Des. 22 (1993) 7.

[42] G. F. Matthews, S. Allen, N. Asakura, J. Goetz, H. Guo, A. Kallenbach, B. Lipschultz, K. McCormick, M. Stamp, U. Samm, P. C. Stangeby, K.-H. Steuer, A. Taroni, B. Unterberg, P. West, “Scaling radiative plasmas to ITER”, J.Nucl.Mater. 241-143 (1997) 450-455.

Appendix

Derivation of equation (3.6) from equation (3.3)

Here is the detailed derivation of equation (3.6) from equation (3.3).

After the Laplace transform, equation (3.3) takes the form:

$$T''(r,s)+\frac{2}{r}T'(r,s)=\frac{s}{\alpha}T(r,s) \qquad \text{(p1)}$$

where $T'(r,s)=\frac{fT(r,s)}{fr}$ and $T''(r,s)=\frac{f^2T(r,s)}{fr^2}$. To solve equation (p1), let's make such a transformation:

$$T(r,s)=\frac{y(r,s)}{r} \qquad \text{(p2)}$$

Inserting equation (p2) into equation (p1), we have:

$$y''(r,s)=\frac{s}{\alpha}y(r,s) \qquad \text{(p3)}$$

The solutions of equation (p3) are readily found to be:

$$y(r,s)=A(s)e^{r\sqrt{s/\alpha}}+B(s)e^{-r\sqrt{s/\alpha}}$$

so that the solution to equation (p1) is:

$$T(r,s)=\frac{y(r,s)}{r}=\frac{1}{r}\left[A(s)e^{r\sqrt{s/\alpha}}+B(s)e^{-r\sqrt{s/\alpha}}\right]$$

where A and B are integral constants. As r [0,R], heat source is on the surface of the sphere, temperature increases from the center to the surface for the irradiation period (heat shock). Based on the physical condition, we take B=0. Thus:

$$T(r,s)=\frac{A(s)}{r}e^{r\sqrt{s/\alpha}} \qquad \text{(p4)}$$

The second boundary condition of equation (3.3) takes the following form after Laplace transformation [Kammash, 1975]:

$$\frac{fT(r,s)}{fr}\Big|_{r=R}=-\frac{\Gamma}{\kappa s}$$

from which we have:

$$A(s) = \frac{\Gamma R^2}{\kappa} \frac{e^{-R\sqrt{s/\alpha}}}{s\left(1 - R\sqrt{s/\alpha}\right)}$$

Thus the solution to equation (p1) takes the form:

$$T(r,s) = \frac{\Gamma R^2}{r\kappa} \frac{\left(-\sqrt{\alpha}/R\right)}{s\left(\sqrt{s} - \sqrt{\alpha}/R\right)} e^{-\frac{R-r}{\sqrt{\alpha}}\sqrt{s}} = \frac{\Gamma R^2}{r\kappa} \frac{ae^{-k\sqrt{s}}}{s\left(a + \sqrt{s}\right)} \qquad \text{(p5)}$$

with $a = -\frac{\sqrt{\alpha}}{R}, k = \frac{R-r}{\sqrt{\alpha}}$

To perform the inverse Laplace transform of equation (p5), we resort the following equation [Beyer, 1978]:

$$L^{-1}\left\{\frac{ae^{-k\sqrt{s}}}{s\left(a+\sqrt{s}\right)}(k \geq 0)\right\} = -e^{ak}e^{a^2 t}erfc\left(a\sqrt{t} + \frac{k}{2\sqrt{t}}\right) + erfc\left(\frac{k}{2\sqrt{t}}\right) \qquad \text{(p6)}$$

where L^{-1} is the inverse Laplace transform operator. Considering that the initial (t=0) temperature is T_0, the final expression of the solution is thus:

$$T(r,t) = T_0 + \frac{\Gamma R^2}{r\kappa}\left[-e^{-\frac{R-r}{R}} e^{\frac{\alpha t}{R^2}} erfc\left(-\frac{\sqrt{\alpha t}}{R} + \frac{R-r}{2\sqrt{\alpha t}}\right) + erfc\left(\frac{R-r}{2\sqrt{\alpha t}}\right)\right] \qquad (3.6)$$

References:

Kammash, T., Fusion Reactor Physics, Ann Arbor Science, 1975, p.392.

Beyer, W. H., (editor), CRC Handbook of Methematical Sciences, 5th Edition, CRC Press, Inc., 1978, p.606.